Cost-Optimal Deployment of Millimeter-Wave Base Stations Under Outage Requirement

Miaomiao Dong, *Member, IEEE,* Minsung Cho, Kangeun Lee, Sungrok Yoon, and Taejoon Kim, *Senior Member, IEEE*

***Abstract*—Today's growth in the volume of wireless devices coupled with the demand for data-intensive use cases has motivated the deployment of millimeter-wave (mmWave) small-cell networks. Although it is true that mmWave networks can carry a large volume of traffic, highly intermittent connectivity and the challenges related to installing many small-cell base stations (BSs) in urban geometry have impeded its progression into practical networks. To cope with these challenges, we present, in this paper, an approach to the mmWave BS deployment (site planning) problem, based on the minimum-deployment-cost criterion that is subject to user equipment (UE) outage constraints. Unlike the prior works, the proposed model captures the randomness of link blockage and signal-to-interference-plus-noise-ratio (SINR) statistics in mmWave networks. We formulate the minimum-cost deployment problem as large-scale integer nonlinear programming (INP). To deal with the combinatorial and coupled nature of the problem, the large-scale INP has approached to devise a suboptimal but efficient algorithm by decomposing it into two subproblems: (i) cell coverage optimization and (ii) minimum subset selection. We provide the solutions to each subproblem as well as theoretical justifications of them. Simulation results that illustrate UE outage guarantees of the proposed BS deployment method are presented. The results reveal that the proposed method uniquely distributes the macro-diversity orders that are distinct from other benchmarks.**

***Index Terms*—Link blockage, outage, minimum-cost base station deployment, integer nonlinear programming, integer linear programming, site planning.**

I. Introduction

Communications in the millimeter-wave (mmWave) bands will play an important role in facilitating the data-intensive fifth-generation (5G) use cases, including real-time machine-type communications, interactive on-line learning, and enhanced augmented reality (EAR). The potential of the mmWave band has made it as one of the important components of future cellular networks [1]–[3]. While it is true that mmWave communications provide very high rate connectivity, contrary to general belief, this does not necessarily translate to high achievable throughput due to significant differences between systems operating in mmWave and legacy sub-6GHz bands.

The initial channel access in the mmWave cellular environment is a very critical task, especially, using directional pencil beams [1], [4], [5]. Particularly, weak diffraction and high attenuation of mmWave propagation make channels vulnerable to *physical blockage*; materials such as brick can attenuate mmWave signals by as much as 40 to 80 dB [6], and the human body can result in a 20 to 35 dB loss [7]. It is evident that under physical blockage the user equipment (UE) cannot access a BS. Even without physical blockage, a UE can still be in blockage due to *UE access-limited blockage*. This is because the number of radio frequency (RF) chains remains limited at the mmWave hybrid massive multiple-input multiple-output (MIMO) BSs, which constrains the number of UEs that can be served concurrently [8]–[13]. Therefore, when the number of active UEs on a time-frequency resource block (RB) is larger than the number of RF chains, UE access-limited blockage occurs. Moreover, accumulated interference from many surrounding BSs can potentially lower the signal-to-interference-plus-noise ratio (SINR) of each UE, causing *SINR outage* [14]. Both blockages and SINR outage will lead to highly intermittent mmWave connectivity.

Previously, the physical blockage has been approached from a macro-diversity point of view [15]–[17]. Macro diversity allows for each UE to be covered by multiple BSs so that whenever a link from a BS is blocked, the link can be restored by another BS that also covers the UE. However, this benefit comes at the price of increasing the number of deployed BSs. The recent growth in the cost of deploying and maintaining large numbers of small-cell BSs is a practical concern that wireless operators are constantly facing [18].

A. Related Work

A pragmatic strategy for BS deployment is to minimize the number of deployed BSs subject to per-UE quality-of-service (QoS) constraints. In this category, BS density optimization [19]–[24] and site-specific BS deployment [25]–[28] methods have been studied. The BS density optimization methods [19]–[24] focus on stochastic geometry to find minimum BS density subject to cell coverage constraints. On the other hand, the site-specific BS deployment methods [25]–[28] find the minimum number of BSs installed on predetermined candidate locations to guarantee UE QoS. The underlying assumption of these works [19]–[28] was omnidirectional and penetrable wave propagation in the sub-6GHz bands, which cannot be extended to mmWave.

M. Dong is with the Department of Electrical Engineering, City University of Hong Kong and the Department of Electrical Engineering and Computer Science, The University of Kansas, Lawrence, KS, USA, emails: miao4600@163.com. T. Kim is with the Department of Electrical Engineering and Computer Science, The University of Kansas, Lawrence, KS, USA, email: taejoonkim@ku.edu. M. Cho, K. Lee, and S. Yoon are with Samsung Electronics, Suwon, Korea, emails: {ke.lee, msstar.cho, sr.eric.yoon}@samsung.com.

This work was supported in part by Samsung. The work of Taejoon Kim was supported in part by the National Science Foundation (NSF) under Grant CNS1955561, and in part by the Office of Naval Research (ONR) under Grant N00014-21-1-2472.

Accounting for mmWave pathloss models, site-specific BS deployment techniques have been studied to maximize line-of-sight (LoS) link distance [29]–[32] and macro diversity orders [33]. While a generic urban geometry was assumed in [29]–[32], BS deployment on a specific Manhattan-type geometry was the focus of [33]. Recently, the site-specific mmWave BS deployment methods that find the minimum number of BSs to ensure the average receive signal power [34], beam alignment reliability [35], and resilience to blockages [36] were studied. Existing mmWave BS deployment algorithms, however, do not account for the randomness of blockages and SINR deviation, caused by the use of directional pencil beams, and fail to provide UE outage guarantees. Given highly intermittent mmWave connectivity, ensuring the UE outage performance is more appropriate than, for example, ensuring the average receive signal power. Thus, a major issue that remains to be addressed is to find an efficient BS deployment algorithm that is cost-optimal and provides UE outage guarantees.

To address the later issues, we formulate, in this paper, the minimum-cost BS deployment problem as large-scale integer nonlinear programming (INP). This aspect has some similarities to the well-investigated problems on optimizing BS sleeping and user association at sub-6GHz bands. These problems were often dealt by formulating INP with the objectives of maximizing network throughput [37], [38] or minimizing the power consumption [26]–[28], [39], [40]. Because large-scale INP is NP-hard and is generally impossible to be optimally solved, devising suboptimal but efficient algorithms was the focus of these approaches, for example, by using greedy heuristics [26]–[28], Lagrangian dual [38], [40], and sequential subproblem formulations [37], [39]. Though these suboptimal treatments were largely benefited from the deterministic link models at sub-6GHz bands, such models and associated problem formulations cannot be extended to the mmWave bands. Although prior approaches [26]–[28], [37]–[40] dealt with INP, they are different from our proposed approach in terms of the objective functions, size of the problem, associated constraints, and thereby, the developed algorithms.

B. Overview of Methodology and Contributions

We present an approach to the problem of mmWave BS deployment, based on the minimum-cost BS deployment criterion that is subject to UE outage constraints taking into account both physical and UE access-limited blockages as well as SINR outage. Our main methodologies and contributions are summarized below.

- We introduce a model for the elementary events of mmWave link outage, which captures the *randomness* of physical blockage, UE access-limited blockage, and SINR outage. The developed model also accounts for directional beam patterns at each BS, as well as random locations of obstacles and UEs. These models facilitate the mathematical formulation of the UE outage constraint.
- We formulate, in this paper, the UE-outage-guaranteed minimum-cost mmWave BS deployment problem as a large-scale INP. The nonlinearity and combinatorial nature of the problem motivate the pursuit of a suboptimal but efficient solution. Moreover, intricate interdependency between the random blockage and outage events makes the UE outage constraint difficult to be incorporated in developing an optimization algorithm. To cope with the difficulties, we conduct a bound analysis and show that the UE outage constraint can be approximated as a set of analyzable constraints. By doing so, we tractably handle the large-scale INP.
- We show that the formulated, large-scale INP can be decomposed into two *separable* subproblems: (i) cell coverage optimization problem and (ii) minimum subset BS selection problem. Since the decomposition is separable, sequentially solving these two subproblems is sufficient. We provide the optimal solutions and theoretical justifications of them. In particular, we show that the second subproblem (minimum subset BS selection problem), which is also large-scale INP, can be transformed into equivalent integer linear programming (ILP) that can be efficiently solved via an existing solver.
- Finally, we evaluate the efficacy of our proposed designs through numerical simulations. It is demonstrated that the proposed scheme provides UE outage guarantees with the minimum-cost deployment, which is not the case of other benchmark schemes [34], [35]. An interesting aspect of the proposed scheme is that the results present a unique distribution of the macro-diversity orders over the network in a way to lower the concentration of macro-diversity orders compared to other benchmark schemes in [34], [35], which is the underlying reason for the improved UE outage guarantee of the proposed scheme.

The rest of the paper is organized as follows. We present the system model in Section II. UE outage analysis is conducted in Section III. The UE outage-guaranteed minimum-cost mmWave BS deployment problem is discussed in Section IV. Section V presents the proposed algorithms. The simulation results and conclusions are provided in Sections VI and VII, respectively. For ease of reference, TABLE I summarizes the main variables which will be used throughout this paper.

II. System Models

We describe an assumed 3D urban geometry, mmWave channel model, and cellular environment under consideration.

A. Urban Geometry

We consider a 3D urban geometry, for example, in Fig. 1, which consists of buildings and streets. The mmWave BSs are mounted on the walls of buildings. We assume that the candidate BS locations are predetermined as red dots in Fig. 1, where the indices of the candidate locations are denoted by $\mathcal{B} = \{1, 2, \ldots, B\}$. Each candidate location has the height $H_{\mathrm{BS},b}, \forall b \in \mathcal{B}$. If a BS is installed at the bth ($b \in \mathcal{B}$) location, $y_b = 1$ and otherwise, $y_b = 0$, where $y_b \in \mathbb{B} = \{0, 1\}$ is the bth entry of the BS deployment vector $\mathbf{y} = [y_1, \ldots, y_B] \in \mathbb{B}^{1\times B}$. Hereafter, a BS installed at the bth candidate location is referred to as "BS b".

Each mmWave BS has its coverage area, called a cell, and serves outdoor active UEs inside the cell in the downlink. Due

TABLE I: List of Main Variables and Their Physical Meanings

Variable	Description
G_{main}	Mainlobe beam gain
G_{side}	Sidelobe beam gain
$H_{\text{BS},b}$	Height of BS b
H_{UE}	Height of UEs
$I_{b,g}$	Interference power from BS b to UE g
L_{grd}	Length of square grid
$n_b(\mathbf{x}_b)$	Number of active UEs without physical blockage in cell b
N_{RF}	Number of RF chains at each BS
$P_{b,g}$	Transmit power of link from BS b to UE g
$p^{\text{blk}}_{b,g}$	Physical blockage probability of link from BS b to UE g
$\rho_{b,g}(\mathbf{x}_b)$	UE access-limited blockage probability from BS b to UE g
$p^{\text{out}}_{b,g}$	Outage probability of the link from BS b to UE g
$\text{PL}_{b,g}$	Pathloss of the link from BS b to grid g
P_{Tx}	Total transmit power of a BS
$R^{\max}$	Maximum link distance for reliable communication
$r_{b,g}$	Distance of the link from BS b to grid g
$r^{\max}_b$	Maximum-link distace in cell b
$\text{SINR}_{b,g}$	SINR of the link from BS b to UE g
$\mathbf{X}\in\mathbb{B}^{B\times G}$	Association matrix
$\mathbf{x}_b\in\mathbb{B}^{1\times G}$	The bth row of $\mathbf{X}$
$\mathbf{y}\in\mathbb{B}^{1\times B}$	BS deployment vector
z	SINR threshold
$\lambda_{\text{UE},g}$	UE density in grid g
ζ_g	UE outage tolerance for grid g
γ	UE access-limited blockage tolerance
σ^2	Noise power

to the physical blockage, the shape of a cell is irregular. To capture the irregularity, the whole outdoor area is divided into G square grids as shown in Fig. 1. We denote the index set of the grids as $\mathcal{G}=\{1,2,\ldots,G\}$. An association indicator $x_{b,g}\in\mathbb{B}$ is introduced, where $x_{b,g}=1$ if the grid $g\in\mathcal{G}$ resides in the cell of BS b, and $x_{b,g}=0$, otherwise. The cell area of BS b is then given by $\sum_g x_{b,g}L^2_{\text{grd}}$, where L_{grd} is the side length of a square grid in Fig. 1. Overlap between cells is allowed so that some UEs in a cell can be simultaneously covered by more than one BS,

$$\sum_{b\in\mathcal{B}} x_{b,g}\geq 1, \tag{1}$$

implying that the macro diversity order is larger than or equal to 1. For notational simplicity, all association indicators $\{x_{b,g}\}$ are collected into an association matrix $\mathbf{X}\in\mathbb{B}^{B\times G}$, where its bth row and gth column entry is $x_{b,g}$.

B. Pathloss Model

Weak diffraction and penetration in the mmWave frequencies make the non-LoS (NLoS) paths suffer from much higher attenuation than the LoS path. As a result, the connectivity of a mmWave link is largely dependent on the LoS path [41]. Hence, in this work, we will focus on the LoS paths for mmWave BS deployment.

In the recent 3GPP 5G specifications (Release 15 [42]), the 28 GHz mmWave band has been allocated as one of the standard bands. Throughout the paper, we will use the LoS pathloss model based on the measurement campaign conducted in an urban area at 28 GHz [4]:

$$\text{PL}_{b,g}=10^{-3.24-2.1\cdot\log_{10}(r_{b,g})-2.0\cdot\log_{10}(28)}, \tag{2}$$

where $\text{PL}_{b,g}$ is the pathloss from BS b to a UE g, and $r_{b,g}$ is the link distance in meters. Herein, the link distance $r_{b,g}$ is limited by a constant $R^{\max}$ ($r_{b,g}\leq R^{\max}$), where $R^{\max}$ is the maximum allowable mmWave link distance for reliable communications.[1] As such, we assume any link with $r_{b,g}>R^{\max}$ is in outage.

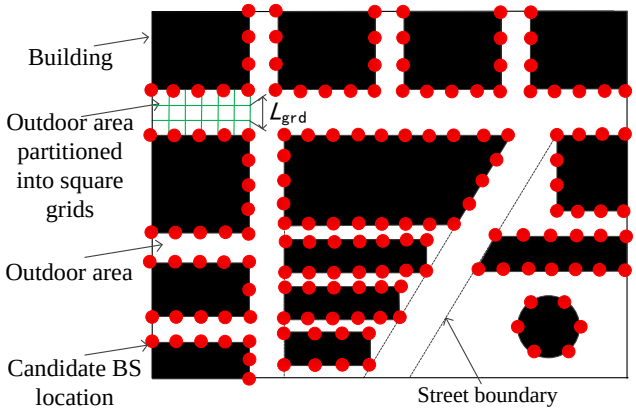

Fig. 1: Bird's-eye view of an exemplary urban street geometry for mmWave BS deployment.

C. Hybrid Array and Beam Pattern

1) Hybrid Analog-Digital Arrays

In the mmWave cellular systems, large-sized antenna arrays are used to generate highly directional narrow beams in order to overcome severe pathloss [1]. Due to power consumption and complexity, analog arrays are typically driven by a limited number of RF chains (N_{RF}). This system is commonly referred to as a hybrid analog-digital mmWave MIMO system [8]–[13], which is the major realization technology for 5G mmWave BS systems. Throughout the paper, we assume that the BSs are equipped with the hybrid mmWave MIMO systems.

2) Beam Pattern

We assume a simplified directional beam pattern at BSs, also known as the cone-shaped beam pattern, as follows

$$G_{\text{BS}}(\theta,\phi)=\begin{cases} G_{\text{main}}, & \text{if } |\theta|\leq\frac{\Delta_\theta}{2},\ |\phi|\leq\frac{\Delta_\phi}{2} \\ G_{\text{side}}, & \text{otherwise}\end{cases}, \tag{3}$$

where G_{main} and G_{side} are the array gains at the mainlode and sidelobe, respectively. Then, $G_{\text{BS}}(\theta,\phi)$ represents the beam gain at elevation θ and azimuth ϕ directions. The Δ_θ and Δ_ϕ in (3) are, respectively, the beamwidths at the elevation θ and azimuth ϕ. Although model (3) is an approximation, it can be shown that (3) closely approach to the actual beam pattern as the array size increases [14], [44], [45]. The BS aligns its beam toward a serving UE to produce beamforming gain G_{main}. In this work, we assume a single antenna UE that generates an omnidirectional receive beam.

D. UE Distribution

We assume that UEs have the same height H_{UE} and $H_{\text{UE}}<H_{\text{BS},b},\forall b\in\mathcal{B}$. To model the UE distribution, we adopt

[1]For example as shown in [43], a 200 meter LoS link at the range of 28GHz frequencies was measured to be extremely unstable for reliable communication, thereby $R^{\max}=200$.

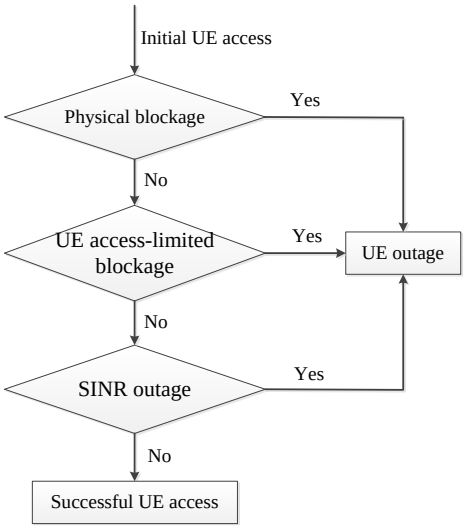

Fig. 2: Logical relationship of the elementary events for link outage.

the non-homogeneous Poisson point process (PPP) [46], [47]. Specifically, given that the partitioned square grids in Fig. 1 are small enough, we treat the users in each grid g to be uniformly distributed with a density $\lambda_{\text{UE},g}$, $g \in \mathcal{G}$ per resource block (RB). A different grid can have different per-RB UE density $\lambda_{\text{UE},g}$. This approximation becomes exact as the square grid reduces to a point, i.e., grid length $L_{\text{grd}} \to 0$.

As aforementioned, the number of simultaneously served UEs on an RB of a hybrid mmWave MIMO system is limited by the number of RF chains N_{RF}. A resource-division multiple access technique can be employed to schedule multiple RBs simultaneously by allocating orthogonal resources, such as time, frequency, and coding blocks (or a combinations of them). Depending on a specific multiple access scheme used, the total number of UEs that can be served on the multiplexed RBs becomes μN_{RF}, where $\mu > 1$ is an RB multiplexing factor. Since μ is implementation-specific, without loss of generality, we focus on, in our paper, a RB. Thus, we develop a BS deployment scheme to guarantee UE access given per-RB UE density $\lambda_{\text{UE},g}, \forall g \in \mathcal{G}$.[2]

III. UE Outage Analysis

In this section, we analyze the statistics of the physical blockage in Section III-A, UE access-limited blockage in Section III-B, and SINR outage in Section III-C. Finally, we formulate in Section III-D the UE outage constraint based on the sequential relationship among the elementary events (i.e., physical blockage, UE access-limited blockage, and SINR outage) as shown in Fig. 2.

A. Physical Blockage Probability

3D ray tracing is adopted to first extract the LoS path from each BS b to each grid g [48]. Physical blockage of the links depends on not only the distance of a link ($r_{b,g} \le R^{\max}$) but also the density and sizes of random obstacles. We assume that the random obstacles on streets are impenetrable cubes. The placement of each obstacle follows a homogeneous PPP with the density λ_{obs} [5]. The physical blockage probability of the link between BS b and grid g is then given by

$$p_{b,g}^{\text{blk}} = \begin{cases} 1-\exp(-\beta r_{b,g}-\alpha), & \text{if } \exists \text{ LoS path} \\ 1 & \text{, otherwise} \end{cases}, \tag{4}$$

where α and β are parameters that depend on the density and sizes of the random obstacles [5]. The variables in (4) follow $\beta = 2\lambda_{\text{obs}} \frac{E[L_{\text{obs}}]+E[W_{\text{obs}}]}{\pi}\eta$ and $\alpha = \lambda_{\text{obs}} E[L_{\text{obs}}]E[W_{\text{obs}}]$, where $E[L_{\text{obs}}]$ and $E[W_{\text{obs}}]$ are the expected length and width of obstacles, respectively, and $\eta = 1 - \int_0^1 \int_0^{sH_{\text{UE}}+(1-s)H_{\text{BS}}} f_h(x)dxds$ where $f_h(x)$ is the probability density function of the height of an obstacle. The expression in (4) clearly reveals that as the obstacle density λ_{obs} and the obstacle sizes grow, the α and β in (4) increase, resulting in a higher blockage probability.

B. UE Access-Limited Blockage Probability

When the mmWave link between a UE and BS is not physically blocked, the UE can attempt channel access to the BS as illustrated in Fig. 2. However, it can still be in blockage because the maximum number of UEs that a BS can simultaneously serve on an RB is limited by N_{RF}, causing UE access-limited blockage. In this subsection, we identify the UE access-limited blockage probability $\rho_{b,g}(\mathbf{x}_b)$ between BS b and a UE in grid g, where $\mathbf{x}_b = [x_{b,1}, \ldots, x_{b,G}] \in \mathbb{B}^{1\times B}$ is the bth row of the association matrix $\mathbf{X}$.

We let $n_b(\mathbf{x}_b)$ be the number of active UEs without physical blockage in the cell area $\sum_g x_{b,g} L_{\text{grd}}^2$ of BS b. Then, the UE access-limited blockage occurs when $n_b(\mathbf{x}_b) > N_{\text{RF}}$. Assuming the equal probability of being successful in channel access of the $n_b(\mathbf{x}_b)$ UEs, given $n_b(\mathbf{x}_b) > N_{\text{RF}}$, the UE g is in UE access-limited blockage with the probability $\frac{n_b(\mathbf{x}_b)-N_{\text{RF}}}{n_b(\mathbf{x}_b)}$. Marginalizing over the events $\{n_b(\mathbf{x}_b) > N_{\text{RF}}\}$, the UE access-limited blockage probability $\rho_{b,g}(\mathbf{x}_b)$ between BS b and a UE in grid g is therefore

$$\rho_{b,g}(\mathbf{x}_b) = \sum_{i:\, i>N_{\text{RF}}} \Pr(n_b(\mathbf{x}_b) = i) \frac{i - N_{\text{RF}}}{i}. \tag{5}$$

To identify $\Pr(n_b(\mathbf{x}_b) = i)$ in (5), we first need to derive the distribution of $n_b(\mathbf{x_b})$. From the independent thinning property of PPP [49], the number of active UEs per grid g, without physical blockage, is Poisson-distributed with the mean $\lambda_{\text{UE},g} L_{\text{grd}}^2 (1 - p_{b,g}^{\text{blk}})$. Because the sum of independent Poisson random variables is still Poisson, $n_b(\mathbf{x}_b)$ is Poission-distributed with the mean

$$E[n_b(\mathbf{x}_b)] = \sum_{g\in\mathcal{G}} x_{b,g} \lambda_{\text{UE},g} L_{\text{grd}}^2 (1 - p_{b,g}^{\text{blk}}). \tag{6}$$

The closed-form expression of (5) is then given by

$$\rho_{b,g}(\mathbf{x}_b) = \sum_{i=N_{\text{RF}}+1}^{+\infty} \frac{E[n_b(\mathbf{x}_b)]^i}{i!} e^{-E[n_b(\mathbf{x}_b)]} \frac{i - N_{\text{RF}}}{i}. \tag{7}$$

Remark 1. *The UE access-limitd blockage $\rho_{b,g}(\mathbf{x}_b)$ in (7) has interdependence between the UE density $\lambda_{UE,g}$ and the*

[2]This means whenever a specific multiple access technique with the multiplexing factor μ is used, the total number of UEs served on the multiplexed RBs is up to a constant scaling factor μ.

cell coverage $\sum_g x_{b,g} L_{grd}^2$ of a BS. Intuitively, if a BS covers a larger number of grids, there are more UEs in the cell requesting channel access, resulting in a higher probability of UE access-limited blockage. The same is true when the UE density $\lambda_{UE,g}$ per-RB grows. Later, we demonstrate this intuition.

C. SINR Outage Probability

As seen in Fig. 2, a UE acquires initial access to BS when it does not experience both physical and UE access-limited blockages. However, even without physical and UE access-limited blockages, accumulated interference from surrounding BSs can cause SINR outage. Denoting the SINR of the link from BS b to a UE g given $\mathbf{y}$ and $\mathbf{X}$ as $\text{SINR}_{b,g}(\mathbf{y},\mathbf{X})$, we denote the SINR outage probability as $\Pr\left(\text{SINR}_{b,g}(\mathbf{y},\mathbf{X})<z|\mathbf{y},\mathbf{X}\right)$, where z is the SINR threshold for reliable communications. Directly analyzing the SINR outage $\{\text{SINR}_{b,g}(\mathbf{y},\mathbf{X}) < z\}$ in the mmWave network is a very difficult task if not impossible to determine. Instead, we resort to a deterministic approach to find a lower bound of $\text{SINR}_{b,g}$ in order to obtain an upper bound of the SINR outage probability $\Pr\left(\text{SINR}_{b,g}(\mathbf{y},\mathbf{X}) < z|\mathbf{y},\mathbf{X}\right)$.

We assume an equal power allocation per UE and write the desired signal power $P_{b,g}(\mathbf{x}_b)$ received at an active UE in grid g from its serving BS b as

$$\begin{aligned} P_{b,g}(\mathbf{x}_b) &= \frac{x_{b,g}P_{\text{TX}}}{\min(n_b(\mathbf{x}_b),N_{\text{RF}})}G_{\text{main}}\text{PL}_{b,g} \\ &\geq \frac{x_{b,g}P_{\text{TX}}}{N_{\text{RF}}}G_{\text{main}}\text{PL}_{b,g} \triangleq \overline{P}_{b,g}(x_{b,g}), \end{aligned} \tag{8}$$

where P_{TX} is the total transmit power of a BS, $\min(n_b(\mathbf{x}_b),N_{\text{RF}})$ is the number of served UEs by BS b, G_{main} follows (3), and $\text{PL}_{b,g}$ is in (2). The last inequality in (8) is due to $\min(n_b(\mathbf{x}_b),N_{\text{RF}}) \leq N_{\text{RF}}$.

We now capture the composite link interference power under the assumption that the mainlobe of a 3D beam in (3) is perfectly aligned with the intended UE and is narrow enough not to cause interference to other UEs. Thus, it is the sidelobe of the beam that causes interference with probability 1. A BS i serving $\min(n_i(\mathbf{x}_i),N_{\text{RF}})$ UEs produces $\min(n_i(\mathbf{x}_i),N_{\text{RF}})$ spatial beams and can impose interference $I_{i,g}(\mathbf{x}_b)$ to a UE in grid g with $\min(n_i(\mathbf{x}_i),N_{\text{RF}})-x_{i,g}$ interfering sidelobes. Note that when $p_{i,g}^{\text{blk}} < 1$ in (4), the interference power $I_{i,g}(\mathbf{x}_b)$ is a Bernoulli random variable with its value either 0 (blocked) or positive (unblocked). Denoting $\mathcal{A}_{i,g}$ as the event that the LoS path between the BS i and UE g is not physically blocked yields

$$\begin{aligned} I_{i,g}(\mathbf{x}_b) &= \mathbb{I}_{\{\mathcal{A}_{i,g}\}}\frac{\left(\min(n_i(\mathbf{x}_i),N_{\text{RF}})-x_{i,g}\right)P_{\text{TX}}}{\min(n_i(\mathbf{x}_i),N_{\text{RF}})}G_{\text{side}}\text{PL}_{i,g} \\ &\leq \left(1-\frac{x_{i,g}}{N_{\text{RF}}}\right)P_{\text{TX}}G_{\text{side}}\text{PL}_{i,g} \triangleq \widehat{I}_{i,g}(x_{i,g}), \end{aligned} \tag{9}$$

where $\mathbb{I}_{\{\mathcal{A}_{i,g}\}}$ is an indicator function: $\mathbb{I}_{\{\mathcal{A}_{i,g}\}} = 1$ if the event $\mathcal{A}_{i,g}$ is true, and $\mathbb{I}_{\{\mathcal{A}_{i,g}\}} = 0$ otherwise. The last inequality in (9) is due to the facts that $\mathbb{I}_{\{\mathcal{A}_{i,g}\}} \leq 1$ and $\min(n_i(\mathbf{x}_i),N_{\text{RF}}) \leq N_{\text{RF}}$. When $\mathbb{I}_{\{\mathcal{A}_{i,g}\}} = 1$ and $n_i(\mathbf{x}_i) \geq N_{\text{RF}}$, the equality holds in (9). This means the bound becomes tight when the physical blockage probability in (4) is relatively low.

Applying the deterministic approach to find the bounds in (8) and (9), the $\text{SINR}_{b,g}$ is readily lower bounded by

$$\text{SINR}_{b,g}(\mathbf{y},\mathbf{X}) \geq \overline{\text{SINR}}_{b,g}(\mathbf{y},\mathbf{X}) \triangleq \frac{\overline{P}_{b,g}(x_{b,g})}{\sigma^2+\sum\limits_{i\in\mathcal{B}} y_i \widehat{I}_{i,g}(x_{i,g})}, \tag{10}$$

where σ^2 is the additive noise power. Thus, the conditional probability of $\overline{\text{SINR}}_{b,g}(\mathbf{y},\mathbf{X}) < z$ given $\mathbf{y}$ and $\mathbf{X}$ is

$$\Pr\left(\overline{\text{SINR}}_{b,g}(\mathbf{y},\mathbf{X})<z|\mathbf{y},\mathbf{X}\right) = \mathbb{I}_{\left\{\overline{\text{SINR}}_{b,g}(\mathbf{y},\mathbf{X})<z|\mathbf{y},\mathbf{X}\right\}}, \tag{11}$$

which is an upper bound of $\Pr\left(\text{SINR}_{b,g}(\mathbf{y},\mathbf{X})<z|\mathbf{y},\mathbf{X}\right)$.

Remark 2. *The lower bound in* (10) *is obtained based on the lower bound of the desired signal power in* (8) *and the upper bound of the interference power in* (9)*. Note that the bound in* (8) *becomes tight when $n_b(\mathbf{x}_b) \approx N_{RF}$; it indeed becomes the equality when $n_b(\mathbf{x}_b) = N_{RF}$. Similarly, the bound in* (9) *becomes tight when $n_b(\mathbf{x}_b) \approx N_{RF}$ as well as when $p_{b,g}^{blk}$ in* (4) *is small. Because the accumulated interference $\sum_{i\in\mathcal{B}} y_i \widehat{I}_{i,g}(x_{i,g})$ in* (10) *is dominated by nearby BSs, these links have low physical blockage probabilities (due to a shorter distance than other links) and thus, a higher chance for the event $\mathcal{A}_{i,g}$ in* (9)*.*

D. UE Outage Constraint

We first identify the UE outage probability for a single link. This model is then extended to the case when there are multiple associated BSs to identify the UE outage constraint

1) Single-Link UE Outage Probability

A link from BS b to a UE g is in outage if one of the following mutually exclusive events occurs as described in the previous subsections: (i) Event $\mathcal{P}_{b,g}$: the channel is physically blocked; (ii) Event $\mathcal{U}_{b,g}$: the channel is physically unblocked, but the UE access-limited blockage occurs; and (iii) Event $\mathcal{S}_{b,g}$: the channel has no blockage and the UE acquires initial access to BS (i.e., $\text{SINR}_{b,g} > 0$), but the SINR outage occurs. Because the three events are mutually exclusive as illustrated in Fig. 2, the outage probability of the single-link is given by

$$p_{b,g}^{\text{Out}} = \Pr(\mathcal{P}_{b,g}) + \Pr(\mathcal{U}_{b,g}) + \Pr(\mathcal{S}_{b,g}). \tag{12}$$

Substituting the physical blockage probability $p_{b,g}^{\text{blk}}$ in (4), UE access-limited blockage $\rho_{b,g}(\mathbf{x}_b)$ in (7), and SINR outage upper bound $\Pr\left(\overline{\text{SINR}}_{b,g}(\mathbf{y},\mathbf{X})<z|\mathbf{y},\mathbf{X}\right)$ in (11) into (12), an upper bound of the single-link outage probability $p_{b,g}^{\text{Out}}$ is given by

$$p_{b,g}^{\text{Out}} \leq p_{b,g}^{\text{blk}} + \left(1-p_{b,g}^{\text{blk}}\right)\rho_{b,g}(\mathbf{x}_b) + \left(1-\rho_{b,g}(\mathbf{x}_b)\right)\widehat{p}_{b,g}^{\text{SINR}}(\mathbf{y},\mathbf{X}), \tag{13}$$

where

$$\widehat{p}_{b,g}^{\text{SINR}}(\mathbf{y},\mathbf{X}) \triangleq \left(1-p_{b,g}^{\text{blk}}\right)\Pr\left(\overline{\text{SINR}}_{b,g}(\mathbf{y},\mathbf{X})<z|\mathbf{y},\mathbf{X}\right) \tag{14}$$

for ease of exposition.

2) UE Outage Constraint

Since a UE g can be covered by multiple BSs (i.e., (1)), the UE outage occurs when all these links are in the outage

simultaneously. Assuming independent outage per link, the UE outage constraint is expressed as

$$\prod_{b=1}^{B}\left[p_{b,g}^{\text{Out}}\right]^{x_{b,g}} \leq \prod_{b=1}^{B}\Big[p_{b,g}^{\text{blk}}+\rho_{b,g}(\mathbf{x}_b)\Big(1-p_{b,g}^{\text{blk}}\Big) +\big(1-\rho_{b,g}(\mathbf{x}_b)\big)\,\widehat{p}_{b,g}^{\text{SINR}}(\mathbf{y},\mathbf{X})\Big]^{x_{b,g}} \leq \zeta_g, \quad (15)$$

where the inequality follows from (13), and $\zeta_g \in (0,1]$ is a UE outage tolerance for gird g. It is clear any $(\mathbf{y},\mathbf{X})$ guaranteeing (15) ensures $\prod_{b=1}^{B}\left[p_{b,g}^{\text{Out}}\right]^{x_{b,g}} \leq \zeta_g$. Taking the logarithm on both sides of (15) yields

$$\sum_{b\in\mathcal{B}} x_{b,g}\log\Big(p_{b,g}^{\text{blk}}+\rho_{b,g}(\mathbf{x}_b)\Big(1-p_{b,g}^{\text{blk}}\Big) +\big(1-\rho_{b,g}(\mathbf{x}_b)\big)\,\widehat{p}_{b,g}^{\text{SINR}}(\mathbf{y},\mathbf{X})\Big) \leq \log\left(\zeta_g\right). \quad (16)$$

Remark 3. *The UE outage tolerance level ζ_g in* (16) *can be determined practically during the BS deployment planning. The implication of imposing* (16) *is that the obtained BS deployment will guarantee successful channel access with a probability larger than $1-\zeta_g$. In urban environments with dense UE distribution, the ζ_g value can be enforced to be small for reliable channel access, while relatively large ζ_g values can be set in rural scenarios. When a grid has no UE, we can set $\zeta_g = 1$ parsimoniously, implying that this grid does not need to be covered by any BSs.*

IV. Minimum-Cost BS Deployment Problem Formulation

The expressions of $\rho_{b,g}(\mathbf{x}_b)$ in (7) and $\Pr\left(\overline{\text{SINR}}_{b,g}(\mathbf{y},\mathbf{X}) < z|\mathbf{y},\mathbf{X}\right)$ in (11) are not fully analyzable, and it is difficult to formulate a solvable optimization problem for our purpose of BS deployment optimization. We thus propose an approximation to replace the (16) with two constraints in Section IV-A. Combined with the BS association constraints presented in Section IV-B, we formulate the minimum-cost mmWave BS deployment problem in Section IV-C.

A. UE Outage Constraint Approximation

About the monotonicity of (16) with respect to the blockage probability $\rho_{b,g}(\mathbf{x}_b)$, we have the following lemma.

Lemma 1. *The logarithmic function in (16)*

$$\log\Big(p_{b,g}^{blk}+\rho_{b,g}(\mathbf{x}_b)\Big(1-p_{b,g}^{blk}\Big)+\big(1-\rho_{b,g}(\mathbf{x}_b)\big)\,\widehat{p}_{b,g}^{SINR}(\mathbf{y},\mathbf{X})\Big)$$

is a monotonically increasing function of the UE access-limited blockage probability $\rho_{b,g}(\mathbf{x}_b)$ in (7)

Proof. See Appendix A. □

We introduce a tolerance level $\gamma \in [0,1]$ to limit the value of $\rho_{b,g}(\mathbf{x}_b)$ in (16) as

$$\rho_{b,g}(\mathbf{x}_b) = \sum_{i=N_{\text{RF}}+1}^{+\infty} \frac{E[n_b(\mathbf{x}_b)]^i}{i!} e^{-E[n_b(\mathbf{x}_b)]}\frac{i-N_{\text{RF}}}{i} \leq \gamma. \quad (17)$$

Replacing the $\rho_{b,g}(\mathbf{x}_b)$ in (16) with γ yields

$$\sum_{b\in\mathcal{B}} x_{b,g}\log\Big(p_{b,g}^{\text{blk}}+\gamma\Big(1-p_{b,g}^{\text{blk}}\Big) +(1-\gamma)\,\widehat{p}_{b,g}^{\text{SINR}}(\mathbf{y},\mathbf{X})\Big) \leq \log\left(\zeta_g\right). \quad (18)$$

Because of Lemma 1 and (17), the left-hand-side of (18) is an upper bound of that in (16) and any $(\mathbf{y},\mathbf{X})$ guaranteeing (18) ensures (16). The (16) can now be approximated by the two constraints (17) and (18).

However, the condition in (17) is still complicate to be directly analyzed as a constraint of an optimization problem. Instead, we find an equivalent, but tractable condition of (17) below.

Lemma 2. *For $\Phi \geq 0$ satisfying $\sum_{i=N_{RF}+1}^{+\infty}\frac{\Phi^i}{i!}e^{-\Phi}\frac{i-N_{RF}}{i} = \gamma$, the inequality in* (17) *is equivalent to the following linear constraint*

$$E[n_b(\mathbf{x}_b)] = \sum_{g\in\mathcal{G}} x_{b,g}\lambda_{UE,g}L_{grd}^2(1-p_{b,g}^{blk}) \leq \Phi. \quad (19)$$

Proof. See Appendix B. □

In Section IV-C, we will take in the two inequalities in (19) and (18) as the UE outage constraint to formulate the BS deployment optimization problem.

B. BS Association Constraints

In this subsection, we list the rules for the elements in the association matrix $\mathbf{X}$. If a BS is installed at the bth candidate location ($y_b = 1$), the association variable is either $x_{b,g} = 1$ or $x_{b,g} = 0$, while if $y_b = 0$, then $x_{b,g} = 0$, yielding

$$x_{b,g} \leq y_b, \quad b \in \mathcal{B},\ g \in \mathcal{G}. \quad (20)$$

Based on the physical blockage model in Section III-A, it is evident that necessary conditions for $x_{b,g} = 1$ are: (i) the link distance $r_{b,g} \leq R^{\max}$ and (ii) the physical blockage probability $p_{b,g}^{\text{blk}} < 1$ in (4), which leads to

$$x_{b,g} \leq \mathbb{I}_{\left\{r_{b,g}\leq R^{\max},\ p_{b,g}^{\text{blk}}<1\right\}},\ b \in \mathcal{B}, g \in \mathcal{G}. \quad (21)$$

Further we assume that the grids closer to a BS have the priority to be associated with the BS. This is to say, whenever a grid g is served by BS b ($x_{b,g} = 1$), other grid $s \in \mathcal{G}$ with $r_{b,s} \leq r_{b,g}$ and $p_{b,s}^{\text{blk}} < 1$ should also be served by the BS b, leading to

$$\mathbb{I}_{\left\{r_{b,s}\leq r_{b,g},\ p_{b,s}^{\text{blk}}<1\right\}} x_{b,g} \leq x_{b,s},\ b \in \mathcal{B}, g, s \in \mathcal{G}. \quad (22)$$

C. Minimum-Cost BS Deployment Problem

Incorporating the BS association constraints in (20)-(22) and UE outage constraints (18), (19) into the minimum-cost BS

deployment criterion gives

$$\min_{\mathbf{y},\mathbf{X}} \ \sum_{b=1}^{B} c_b y_b \tag{23a}$$

$$\text{subject to} \ \ x_{b,g} \le y_b, \tag{23b}$$

$$x_{b,g} \le \mathbb{I}_{\left\{r_{b,g}\le R^{\max},\, p^{\text{blk}}_{b,g}<1\right\}}, \tag{23c}$$

$$\mathbb{I}_{\left\{r_{b,s}\le r_{b,g},\, p^{\text{blk}}_{b,s}<1\right\}} x_{b,g} \le x_{b,s}, \tag{23d}$$

$$E[n_b(\mathbf{x}_b)] \le \Phi, \tag{23e}$$

$$\sum_{b\in\mathcal{B}} x_{b,g}\log\Big(p^{\text{blk}}_{b,g}+\gamma\left(1-p^{\text{blk}}_{b,g}\right) + (1-\gamma)\,\widehat{p}^{\,\text{SINR}}_{b,g}(\mathbf{y},\mathbf{X})\Big)\le \log\left(\zeta_g\right), \tag{23f}$$

$$y_b\in\{0,1\},\ x_{b,g}\in\{0,1\},\ \ \forall b\in\mathcal{B},\ g\in\mathcal{G},$$

where c_b in (23a) is the BS installation cost at location $b \in \mathcal{B}$. The objective in (23a) is to minimize the cost for deploying BSs by jointly optimizing the *BS deployment vector* $\mathbf{y} \in \mathbb{B}^{1\times B}$ and *association matrix* $\mathbf{X} \in \mathbb{B}^{B\times G}$. Because of the nonlinear constraint (23f) with respect to the binary vector $\mathbf{y}$ and matrix $\mathbf{X}$, the problem in (23) is INP, which is excessively complex to be directly solvable [50]. More specifically, directly searching for the optimal solution needs to evaluate all $2^{B\times(G+1)}$ combinations of $(\mathbf{y}, \mathbf{X})$, which is prohibitive for relatively large B and G (e.g., $B \ge 100$ and $G \ge 100$). In the next subsection, we address this challenge and propose a low-complexity approach to optimally solve the problem (23).

V. Minimum-Cost BS Deployment Algorithm

In this section, we find an optimal solution to the problem in (23). The key to optimally solving (23) lies in decomposing it into two *separable* subproblems: (i) cell coverage optimization problem, which finds a feasible association matrix $\mathbf{X}$ for the constraints in (23b)-(23f) as a function of the BS deployment vector $\mathbf{y}$, and (ii) minimum-cost subset BS selection problem, which finds the minimum-cost $\mathbf{y}$ to guarantee the UE outage constraint in (23f). The main motivation of this approach is that the objective $\sum_{b=1}^{B} c_b y_b$ in (23) is independent of $\mathbf{X}$, and thus, any feasible $\mathbf{X}$ (i.e., satisfying (23b)-(23f)) is optimal to the problem. The cell coverage optimization subproblem is first discussed below.

A. Cell Coverage Optimization

As a starting point, we introduce the following proposition showing a monotonic relationship between the macro diversity order in (1) and the left-hand-side of (23f).

Lemma 3. *For a fixed BS deployment vector* $\mathbf{y}$*, the left-hand-side of* (23f) *is a monotonically decreasing function of the macro diversity order* $\sum_{b\in\mathcal{B}} x_{b,g}$ *in* (1).

Proof. See Appendix C. □

This lemma reveals that for a fixed $\mathbf{y}$ the left-hand-side of (23f) is minimized by maximizing the macro diversity order $\sum_b x_{b,g}$ of each grid. Hence, a feasible association matrix $\mathbf{X}$ satisfying (23b)-(23f) for a given $\mathbf{y}$, can be obtained by maximizing the macro diversity order $\sum_b x_{b,g}$ subject to the constraints in (23b)-(23e). To express the feasible $\mathbf{X}$ as a function of $\mathbf{y}$, we introduce an auxiliary variable $\Lambda_{b,g} \in \mathbb{B}$, referred to here as a coverage indicator, associated with the candidate location $b\in\mathcal{B}$ and the grid $g\in\mathcal{G}$, such that

$$x_{b,g} = y_b\Lambda_{b,g}, \tag{24}$$

where $\Lambda_{b,g} = 1$ if a candidate BS location $b \in \mathcal{B}$ (regardless whether $y_b = 1$ or $y_b = 0$) covers the grid g, and $\Lambda_{b,g} = 0$ otherwise. The objective of maximizing the macro diversity order of all grids for a given $\mathbf{y}$ can be transformed to the objective of maximizing the cell coverage of each candidate location b as follows,

$$\max_{\mathbf{X}}\sum_{g=1}^{G}\sum_{b=1}^{B}x_{b,g}=\max_{\mathbf{X}}\sum_{b=1}^{B}\sum_{g=1}^{G}x_{b,g}=\sum_{b=1}^{B}y_b\max_{\mathbf{\Lambda}_b}\sum_{g=1}^{G}\Lambda_{b,g}, \tag{25}$$

where the first equality follows from the fact that changing the order of summations does not alter the optimality, and the second equality is due to $x_{b,g} = y_b\Lambda_{b,g}$ and the fact that $\mathbf{y}$ is fixed, where $\sum_{g=1}^{G}\Lambda_{b,g}$ is the cell coverage of the candidate location b and $\mathbf{\Lambda}_b = [\Lambda_{b,1}, \ldots, \Lambda_{b,G}] \in \mathbb{B}^{1\times G}$. Motivated by (25), we find the maximum cell coverage of each candidate location b based on the BS coverage (23b)-(23d) and UE access-limited blockage (23e) constraints, leading to the cell coverage optimization problem:

$$\max_{\mathbf{\Lambda}_b} \ \sum_{g=1}^{G}\Lambda_{b,g}, \quad \forall b\in\mathcal{B} \tag{26a}$$

$$\text{subject to} \ \ \Lambda_{b,g} \le \mathbb{I}_{\{r_{b,g}\le R^{\max}, p^{\text{blk}}_{b,g}<1\}}, \tag{26b}$$

$$\mathbb{I}_{\left\{r_{b,s}\le r_{b,g},\, p^{\text{blk}}_{b,s}<1\right\}}\Lambda_{b,g} \le \Lambda_{b,s}, \tag{26c}$$

$$E[n_b(\mathbf{\Lambda}_b)] \le \Phi, \tag{26d}$$

$$\Lambda_{b,g}\in\{0,1\},\ \ \forall\, g\in\mathcal{G},$$

where

$$E[n_b(\mathbf{\Lambda}_b)]=\sum_{g\in\mathcal{G}}\Lambda_{b,g}\lambda_{\text{UE},g}L^2_{\text{grd}}(1-p^{\text{blk}}_{b,g}). \tag{27}$$

The association constraint (23b) is omitted because the construction in (24) already implies (23b). We note that all constraints in (26) are consistent with those in (23) except for that it excludes the UE outage constraint in (23f) and $x_{b,g}$ is changed to $\Lambda_{b,g}$. Without loss of optimality, we relegate $E[n_b(\mathbf{x}_b)] \le \mathbf{\Phi}$ in (23e) to $E[n_b(\mathbf{\Lambda}_b)] \le \mathbf{\Phi}$ because $E[n_b(\mathbf{\Lambda}_b)] \le \mathbf{\Phi}$ implies $E[n_b(\mathbf{x}_b)] \le \mathbf{\Phi}$.

Since the coverage maximization at each candidate location is separable and the grids closer to a candidate location have the priority to be associated with the BS due to (26c), pursuing $\max_{\mathbf{\Lambda}_b}\sum_{g=1}^{G}\Lambda_{b,g}$, $\forall b\in\mathcal{B}$ in (26) is equivalent to finding the maximum-link distance $r_b^{\max}$, $\forall b\in\mathcal{B}$:

$$r_b^{\max} \ = \max_{\mathbf{\Lambda}_b} \ \Lambda_{b,g}r_{b,g} \tag{28}$$

$$\text{subject to:}\ \ (26b),\ (26c),\ (26d),\ r_{b,g}\le R^{\max},\ \forall\, g\in\mathcal{G}.$$

Accounting for the constraints in (26b) and (26c), it is clear that as the BS b covers more grids (i.e., $\sum_{g=1}^{G}\Lambda_{b,g}$ increases) the objective in (28) increases. From (27) it is also clear that

$E[n_b(\mathbf{\Lambda}_b)]$ in (26d) is a monotonically increasing function of $\sum_{g=1}^{G}\Lambda_{b,g}$. Hence the $r_b^{\max}$ in (28) is attained either when (i) $E[n_b(\mathbf{\Lambda}_b)]=\Phi$ and $r_b^{\max}<R^{\max}$ or (ii) $E[n_b(\mathbf{\Lambda}_b)]\leq\Phi$ and $r_b^{\max}=R^{\max}$.

Based on the above observations, optimal $r_b^{\max}$ in (28) can be efficiently searched via iterative feasibility testing. Specifically, a bisection method for solving (28) is presented in Algorithm 1. At each iteration with a given $r_b^{\max}$, Algorithm 1 exploits the facts that the constraints (26b) and (26c) determine which grids are associated with the candidate location b, while the UE access-limited constraint (26d) and $R^{\max}$ examine the feasibility of the $r_b^{\max}$. The Step 5 of Algorithm 1 identifies the indicator $\Lambda_{b,g}$ such that $\Lambda_{b,g}=1$ if $r_{b,g}\leq r_b^{\max}$ and $p_{b,g}^{\text{blk}}<1$, and $\Lambda_{b,g}=0$ otherwise, $\forall b\in\mathcal{B}$, $\forall g\in\mathcal{G}$. It also exploits the constraint (26c); provided $\Lambda_{b,g}=1$, for other grid $s\in\mathcal{G}$ we have $\Lambda_{b,s}=1$ if $r_{b,s}\leq r_{b,g}$ and $p_{b,s}^{\text{blk}}<1$, and $\Lambda_{b,s}=0$ otherwise. Algorithm 1 requires exactly $\lceil\log_2(R^{\max}/\epsilon)\rceil$ iterations.

Algorithm 1 Solving max coverage problem in (28), $\forall b\in\mathcal{B}$

1: **Initialize** Lower bound $LB=0$, upper bound $UB=R^{\max}$, tolerance $\epsilon>0$,
2: **for** $b=1:B$ **do**
3: **while** $UB-LB>\epsilon$ **do**
4: $MD=\frac{LB+UB}{2}$; $r_b^{\max}=MD$
5: Determine $\mathbf{\Lambda}_b$ using (26b), (26c)
6: **if** $E[n_b(\mathbf{\Lambda}_b)]\leq\Phi$ in (26d) **then**
7: Update $LB=MD$
8: **else**
9: Update $UB=MD$
10: **end if**
11: **end while**
12: **end for**
13: **return** $r_b^{\max},\forall b\in\mathcal{B}$.

Once $r_b^{\max}$, $\forall b\in\mathcal{B}$, in (28) are determined, we obtain the optimal coverage indicators $\Lambda_{b,g}^{\star},\forall b\in\mathcal{B},\forall g\in\mathcal{G}$, based on Step 5 of Algorithm 1. Then, the association matrix $\mathbf{X}$ is constructed as a function of the given $\mathbf{y}$ according to

$$x_{b,g}^{\star}=y_b\Lambda_{b,g}^{\star},\ \ \forall b\in\mathcal{B},\ \forall g\in\mathcal{G}. \tag{29}$$

We denote the optimal $\mathbf{X}$ obtained in (29) as $\mathbf{X}_{\mathbf{y}}^{\star}$. Note that for a fixed $\mathbf{y}$, the optimized $\mathbf{X}_{\mathbf{y}}^{\star}$ in (29) satisfies the constraints (23b)-(23e) and minimizes the left-hand-side of (23f).

B. Minimum-Cost Subset BS Selection

The remaining task is to find the $\mathbf{y}$ that minimizes the object in (23) to guarantee the UE outage constraint in (23f), which leads to the second subproblem:

$$\min_{\mathbf{y}}\ \sum_{b=1}^{B}c_by_b \tag{30a}$$

$$\text{subject to}\ \sum_{b\in\mathcal{B}}x_{b,g}\log\Big(p_{b,g}^{\text{blk}}+\gamma\left(1-p_{b,g}^{\text{blk}}\right)+(1-\gamma)\,\widehat{p}_{b,g}^{\text{SINR}}(\mathbf{y},\mathbf{X}_{\mathbf{y}}^{\star})\Big)\leq\log\left(\zeta_g\right),\tag{30b}$$

$$y_b\in\{0,1\},\ \forall b\in\mathcal{B}.$$

Using (10), (11), and (14), the $\widehat{p}_{b,g}^{\text{SINR}}(\mathbf{y},\mathbf{X}_{\mathbf{y}}^{\star})$ in (30b) can be rewritten as

$$\begin{aligned}\widehat{p}_{b,g}^{\text{SINR}}(\mathbf{y},\mathbf{X}_{\mathbf{y}}^{\star})&\overset{(a)}{=}(1-p_{b,g}^{\text{blk}})\mathbb{I}\left\{\frac{\overline{P}_{b,g}(y_b\Lambda_{b,g}^{\star})}{\sigma^2+\sum_{i\in\mathcal{B}}y_i\widehat{I}_{i,g}(y_i\Lambda_{i,g}^{\star})}<z\right\}\\&\overset{(b)}{=}(1-p_{b,g}^{\text{blk}})\mathbb{I}\left\{\frac{y_b\overline{P}_{b,g}(\Lambda_{b,g}^{\star})}{\sigma^2+\sum_{i\in\mathcal{B}}y_i\widehat{I}_{i,g}(\Lambda_{i,g}^{\star})}<z\right\}\\&=\tilde{p}_{b,g}^{\text{SINR}}(\mathbf{y}),\end{aligned}\tag{31}$$

where (a) is because of (29), and (b) is due to the fact that $\overline{P}_{b,g}(y_b\Lambda_{b,g}^{\star})=0$ if $y_b=0$ and $y_i\widehat{I}_{i,g}(y_i\Lambda_{i,g}^{\star})=y_i\widehat{I}_{i,g}(\Lambda_{i,g}^{\star})$. By doing so, we manipulate the UE outage constraint in (30b) so that it only depends on $\mathbf{y}$. The problem in (30) is therefore reformulated as

$$\min_{\mathbf{y}}\ \sum_{b=1}^{B}c_by_b \tag{32a}$$

$$\text{subject to}\ \sum_{b=1}^{B}y_b\Lambda_{b,g}^{\star}\log\Big(p_{b,g}^{\text{blk}}+\gamma\left(1-p_{b,g}^{\text{blk}}\right)+(1-\gamma)\,\tilde{p}_{b,g}^{\text{SINR}}(\mathbf{y})\Big)\leq\log\left(\zeta_g\right),\tag{32b}$$

$$y_b\in\{0,1\},\forall b\in\mathcal{B},$$

which is INP because of the nonlinear constraint in (32b).

We show in the following lemma that the constraint in (32b) can be transformed to a set of linear constraints so that the problem in (32) is converted to integer linear programming (ILP).

Lemma 4. *Suppose auxiliary variables $s_{b,g}\in\mathbb{B}$, $\forall b\in\mathcal{B}$, $\forall g\in\mathcal{G}$, which is determined to satisfy the indicator function in* (31) *of $\tilde{p}_{b,g}^{SINR}(\mathbf{y})$:*

$$\mathbb{I}\left\{\frac{y_b\overline{P}_{b,g}(\Lambda_{b,g}^{\star})}{\sigma^2+\sum_{i\in\mathcal{B}}y_i\widehat{I}_{i,g}(\Lambda_{i,g}^{\star})}<z\right\}=1-s_{b,g}.\tag{33}$$

The constraint in (32b) is equivalent to the following set of linear constraints,

$$s_{b,g}\leq y_b\Lambda_{b,g}^{\star},\ \ s_{b,g}\in\mathbb{B},\tag{34a}$$

$$\sigma^2+\sum_{i\in\mathcal{B}}y_i\widehat{I}_{i,g}(\Lambda_{b,g}^{\star})\geq\frac{y_b\overline{P}_{b,g}(\Lambda_{b,g}^{\star})}{z}-s_{b,g}M_{b,g},\tag{34b}$$

$$\sigma^2+\sum_{i\in\mathcal{B}}y_i\widehat{I}_{i,g}(\Lambda_{i,g}^{\star})<\frac{y_b\overline{P}_{b,g}(\Lambda_{b,g}^{\star})}{z}+\left(1-s_{b,g}\right)M_{b,g},\tag{34c}$$

$$\sum_{b\in\mathcal{B}}s_{b,g}\log\Big(p_{b,g}^{blk}+\gamma(1-p_{b,g}^{blk})\Big)\leq\log\left(\zeta_g\right),\tag{34d}$$

where z is the link SINR threshold in (31) *and $M_{b,g}=2\sigma^2+\sum_{i\in\mathcal{B}}\widehat{I}_{i,g}(\Lambda_{i,g}^{\star})$.*

Proof. See Appendix D. □

TABLE II: Simulation Parameters

Variables and Description	Values
BS height	$H_{\text{BS}} = 10$ m
UE height H_{UE}	$H_{\text{UE}} = 1.5$ m
Square grid length L_{grd}	$L_{\text{grd}} = 5$ m
Numbers of candidate BS locations	$B = 240/184/130$
Numbers of grids	$G = 7393$
Parameters for physical blockage in (4)	$\alpha = 0.08$, $\beta = 0.08$
Number of RF chains N_{RF}	$N_{\text{RF}} = 12$
Maximum link distance $R^{\max}$	$R^{\max} = 200$ m [43]
Link SINR threshold z	$z = 1$
UE outage tolerance	$\zeta_g = 0.05, \forall g \in \mathcal{G}$
Mainlobe and sidelobe beam gain	$G_{\text{main}} = 15$ dB and $G_{\text{side}} = -9$ dB [45]
BS transmit power	$P_{\text{Tx}} = 1$ Watt [52]
Noise power σ^2	$\sigma^2 = -104.5$ dBm [53]
Tolerance ϵ in Algorithm 1	$\epsilon = 0.1$

Lemma 4 allows us to transform the INP in (32) to ILP:

$$\begin{aligned} \min_{\mathbf{y}} \quad & \sum_{b=1}^{B} c_b y_b \\ \text{subject to} \quad & \text{(34a), (34b), (34c), (34d),} \\ & y_b \in \{0,1\}, \forall b \in \mathcal{B}. \end{aligned} \tag{35}$$

C. Overall Algorithm

We now present our overall framework for finding the optimal solution to the minimum-cost BS deployment problem in (23). The optimal $\{\Lambda^{\star}_{b,g}\}$, $\forall b \in \mathcal{B},\ \forall g \in \mathcal{G}$, are obtained by Algorithm 1 that solves the problem in (28) (equivalently, (26)). After attaining the optimal association matrix $\mathbf{X}^{\star}_{\mathbf{y}}$ as a function of the BS deployment vector $\mathbf{y}$, the problem in (35) is solved to obtain the minimum-cost BS deployment $\mathbf{y}$. We notice that the ILP in (35) is a standard integer programming, which can be globally solved by the branch-and-bound (B&B) method [50]. Since it is a standard procedure and there are numerous efficient solvers (e.g., Gurobi [51]), we omit the details here.

1) Nulling Variables for Complexity Reduction

A drawback of the linearization in (35) (respectively, Lamma 4) is that binary auxiliary variables $s_{b,g}, \forall b \in \mathcal{B}, g \in \mathcal{G}$ are additionally introduced, which will stymie the computation of the B&B method. Nevertheless, based on the fact that $s_{b,g} \leq y_b \Lambda_{b,g}$ in (41) in Appendix D, one can reduce the number of variables by setting $s_{b,g} = 0$ when $\Lambda^{\star}_{b,g} = 0$. Moreover, in the B&B method, one can effectively reduce the number of branches; when an element y_b in $\mathbf{y}$ is branched into $y_b = 0$, values of the auxiliary variables $s_{b,g}, \forall b$, becomes zero. In this way, the increased computational complexity due to the introduced $\{s_{b,g}\}$ is reasonably reduced.

VI. Simulation Studies

In this section, we numerically evaluate the proposed BS deployment scheme in terms of the deployment cost, computational complexity, and UE outage performance. The geometry in Fig. 3 with dimension 390 m $\times$ 735 m is considered to evaluate the performance of the proposed BS deployment scheme. Different numbers of candidate BS locations (i.e., $B = 240, B = 184, B = 130$ in Fig. 3(b)) are considered to evaluate the impact of BS candidate number B on the network deployment cost. Specific parameters of the geometry in Fig. 3 and the considered mmWave systems are summarized in TABLE II. Different grid g could have different UE density $\lambda_{\text{UE},g}$. For ease of exposition, we divide the area into five distinct regions as shown in Fig. 3(b) and assume that the grids in the same region have the same UE density, where the UE density of the ith region is described by $\lambda^{(i)}_{\text{UE}} = (2i+2) \times 10^{-4}$, $i = 1, \ldots, 5$. Based on the parameters in TABLE II, there are on average 165 active UEs for initial access per RB. Considering the fact that the cost c_b in (23a) of installing a BS in an area with higher UE density (e.g., urban area) is, in general, more costly than that of lower density (e.g., rural area), we set the installation cost c_b in the ith region as $0.2i$, $i = 1, \ldots, 5$.

A. Benchmark Algorithms

We will compare our proposed BS deployment algorithm against the site-specific mmWave BS deployment strategies below.

- *Macro Diversity-Constrained Approach (MDCA)*: The MDCA is formed by minimizing the BS deployment cost in (23a) and by requiring each grid to be covered by at least two BSs:

$$\begin{aligned} \min_{\mathbf{y}} \quad & \sum_{b=1}^{B} c_b y_b \\ \text{subject to} \quad & \sum_{b=1}^{B} x_{b,g} \geq 2,\ \forall g \in \mathcal{G}. \end{aligned} \tag{36}$$

  The constraint provides resilience to the physical blockage. The MDCA in (36) is ILP, and thus can be efficiently solved by using available solvers.
- *Average Signal Strength-Guaranteed Approach (ASSGA) in [34]*: The underlying idea of ASSGA is to distribute BSs to guarantee a certain level of average received signal strength (RSS). The ASSGA is therefore formed by adding a threshold for the RSS of each UE to the MDCA in (36):

$$\begin{aligned} \min_{\mathbf{y}} \quad & \sum_{b=1}^{B} c_b y_b \\ \text{subject to} \quad & \sum_{b=1}^{B} x_{b,g} \geq 2,\ \forall g \in \mathcal{G} \\ & \frac{1}{\sum_{b=1}^{B} x_{b,g}} \sum_{b=1}^{B} x_{b,g} \text{RSS}_{b,g} \geq \text{RSS}_{\text{th}}, \forall g \in \mathcal{G}, \end{aligned} \tag{37}$$

  where $\text{RSS}_{b,g} = P_{b,g} + G_{\text{main}} - \text{PL}_{b,g}(r_{b,g})$ in dB is the RSS of the link from BS b to grid g with distance $r_{b,g}$, and the RSS threshold is set to $\text{RSS}_{\text{th}} = -90$ dB. The problem in (37) is solved by using the algorithm proposed in [34].
- *Blockage-Guaranteed Greedy Approach (BGGA)*: In this benchmark, we focus on a strategy that provides blockage tolerance. This is obtained by replacing the UE outage constraint (23f) in (23) with

$$\sum_{b \in \mathcal{B}} x_{b,g} \log\left(p^{\text{blk}}_{b,g} + \gamma \left(1 - p^{\text{blk}}_{b,g}\right)\right) \leq \log\left(\zeta_g\right),\ \forall g \in \mathcal{G}. \tag{38}$$

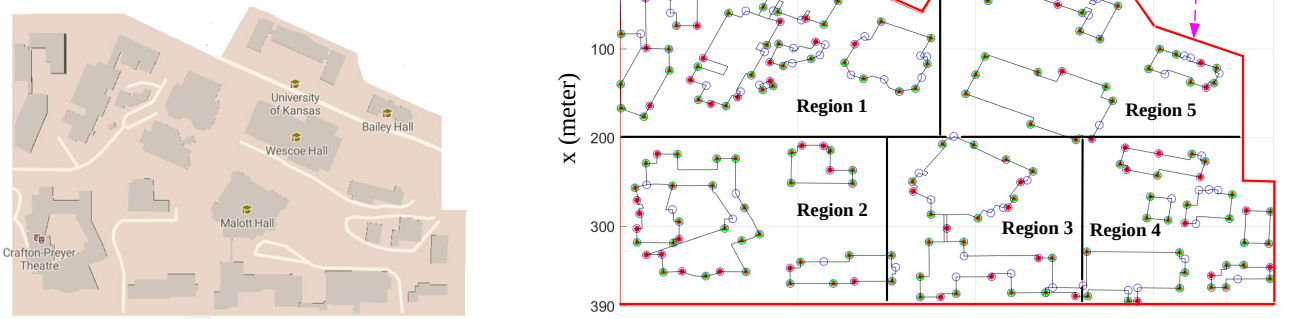

(a) 3D campus of the University of Kansas.

(b) Illustration of campus with different number B of candidate BS locations (i.e., $B=240$ (blue circles), $B=184$ (blue circles+red$*$), and $B=130$ (blue circles+red$*$+green triangle)) on the building walls and the square grids partitioning the outdoor campus. Five regions with the different active UE densities: the UE density at the ith region is $\lambda_{\mathrm{UE},g}^{(i)}=(2i+2)\times 10^{-4}$, $i=1,2,\ldots,5$.

Fig. 3: Campus map of the University of Kansas for outdoor mmWave BS deployment evaluation.

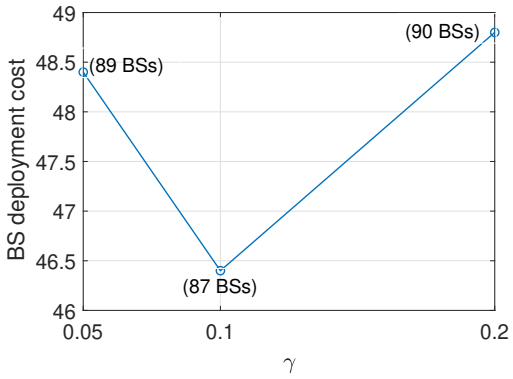

Fig. 4: Minimum BS deployment cost under different γ.

Similar to the proposed algorithm, we decompose (38) into the two separable subproblems. The BS coverage optimization subproblem is first solved by the algorithm in Section-V-A. To solve the minimum-cost subset BS selection subproblem with the constraint in (38), we adopt the greedy algorithm (GA) proposed in [35]. In the GA, a new BS is added per iteration that guarantees the constraint (38) while minimizing the BS deployment cost. The iteration ends when (38) holds for all G grids.

B. Performance Evaluation

In this subsection, we present the BS deployment results obtained by the proposed scheme and the benchmarks MDCA, ASSGA, and BGGA. Using these results, we compare and contrast the link SINR and UE outage performance.

1) Impact of γ on BS Deployment Cost

Different values of UE access-limited blockage tolerance $\gamma \in [0,1]$ in (17) will lead to different solutions to the problem (23). In this part of the simulation, we study the interdependency between the γ and its corresponding objective value $\sum_{b=1}^{B} c_b y_b^\star$ in Fig. 6 for $\gamma \in \{0.05, 0.1, 0.2\}$. It is noticed that as the γ grows from 0.05 to 0.2, the objective value first decreases and then increases. The minimum objective value $\sum_{b=1}^{B} c_b y_b^\star = 46.4$ is achieved when $\gamma = 0.1$. This is because, as stated in Remark 1, a larger γ allows each BS to cover a more number of grids. This leads to a larger macro diversity order to each grid, but also leads to more serious UE access-limited blockage and SINR outage. When γ grows from 0.05 to 0.1, the macro diversity benefits dominate the latter, and this is reversed when γ further increases to 0.2. When $\gamma \geq 0.3$, the problem (23) becomes infeasible due to a relatively high tolerance on UE access-limited blockage probability. Based on the above observation, in what follows, we evaluate the proposed algorithm (by setting $\gamma = 0.1$) with the selected benchmarks, i.e., MDCA, ASSGA, and BGGA.

2) BS Coverage Maximization

Fig. 4 presents the maximum link distance $r_b^{\max}$ (meters) values of (28) in blue at ten different candidate BS locations, obtained by Algorithm 1. Because the Region 5 has the highest UE density, those candidate locations have relatively small coverage radii[3] due to the increased UE access-limited blockage. The candidate locations in the open areas of Regions 1 and 2 are LoS-visible to many grids and most of the maximum link distances are larger than 150 meters due to the relatively low UE density. This observation reveals that the maximum link distance depends on both the UE density and the nearby geometry.

[3]Those values are 96, 113, 126, and 200 meters in Fig. 4. Since the BS candidate at the boundary of Region 5 is LoS-visible to a limited number of grids, it has the maximum link distance 200 meters.

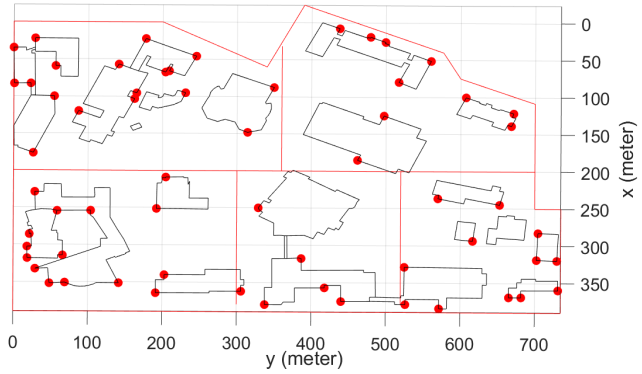

(a) MDCA scheme, 61 deployed BSs with cost $\sum_{b=1}^{B} c_b y_b = 32.8$.

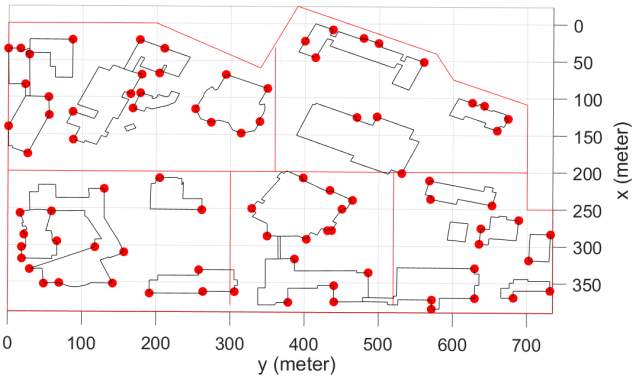

(b) ASSGA scheme, 84 deployed BSs with cost $\sum_{b=1}^{B} c_b y_b = 45$.

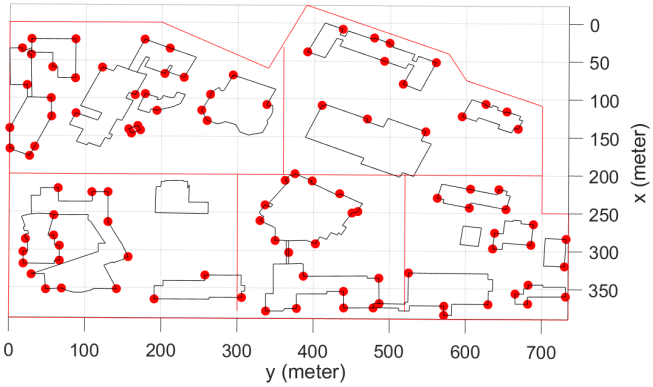

(c) BGGA scheme, 102 deployed BSs with cost $\sum_{b=1}^{B} c_b y_b = 55$.

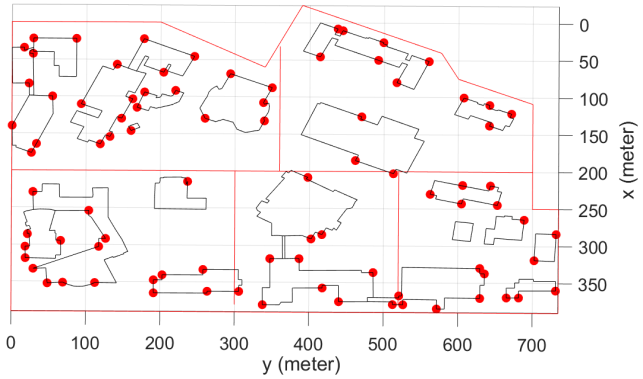

(d) Proposed scheme, 87 deployed BSs with cost $\sum_{b=1}^{B} c_b y_b = 46.4$.

Fig. 5: BS deployment results of the benchmarks MDCA, ASSGA, BGGA, and the proposed scheme for $B = 240$ candidate locations.

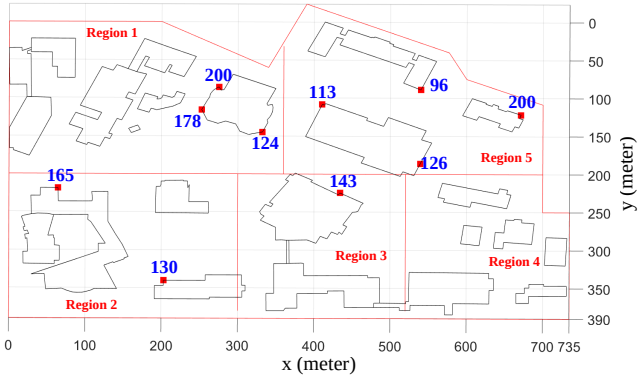

Fig. 6: Maximum link distance $r_b^{\max}$ in (28) for 10 candidate BS locations. The $r_b^{\max}$ values are best represented by the blue fonts.

3) BS Deployment Cost

Given $B = 240$ candidate BS locations shown as blue circles in Fig. 3(b), the BS deployment results of the proposed method and the benchmark MDCA, ASSGA, and BGGA, are displayed in Fig. 5. The numbers of the deployed BSs of the proposed, MDCA, ASSGA, and BGGA schemes are given by 87, 61, 84, and 102, respectively. The proposed scheme and BGGA yield larger numbers of deployed BSs due to the UE access-limited blockage constraint, in which a BS b has a maximum link distance $r_b^{\max} \leq R^{\max}$ as in Fig 4 and can only cover a limited number of grids. Among the four strategies, the MDCA in Fig. 5(a) deploys the least number of BSs because the MDCA criterion merely focuses on extending the LoS link distance to ensure the macro diversity order constraint in (36). In contrast, ASSGA, BGGA, and the proposed scheme attempt to evenly distribute the BSs. This is because the average RSS constraint (37) in ASSGA, the blockage constraint (38) in BGGA, and the UE outage constraint (23f) in the proposed scheme control the link distance so that a UE far from its serving BS experiences unsatisfactory link performance. Observing the constraints in (38) and (23f), it is evident that the BS deployment by the proposed scheme is feasible to the BGGA. However, this is not observed from Figs 5(c) and 5(d) because the BGGA algorithm in [35] is based on a greedy approach.

4) SINR Performance

Given the BS deployment results in Fig. 5, we collect each link's $\text{SINR}_{b,g}(\mathbf{y}^\star, \mathbf{X}^\star)$ values for 50 random realizations of UEs. The cumulative distribution functions (CDFs) of the collected $\{\text{SINR}_{b,g}(\mathbf{y}^\star, \mathbf{X}^\star)\}$ of the proposed and benchmark schemes are displayed in Fig. 7, where $F(x)$ denotes the CDF and x is the abscissa (i.e., SINR). For the proposed scheme,

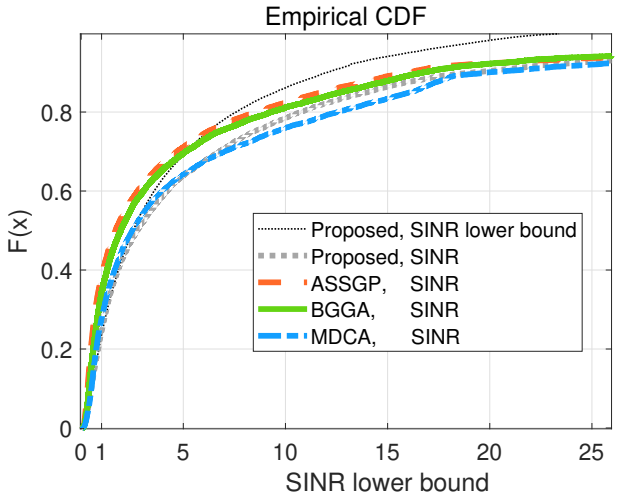

Fig. 7: CDF of the links' SINR and its SINR lower bound $\overline{\text{SINR}}_{b,g}(\mathbf{y}^\star, \mathbf{X}^\star)$ in (10).

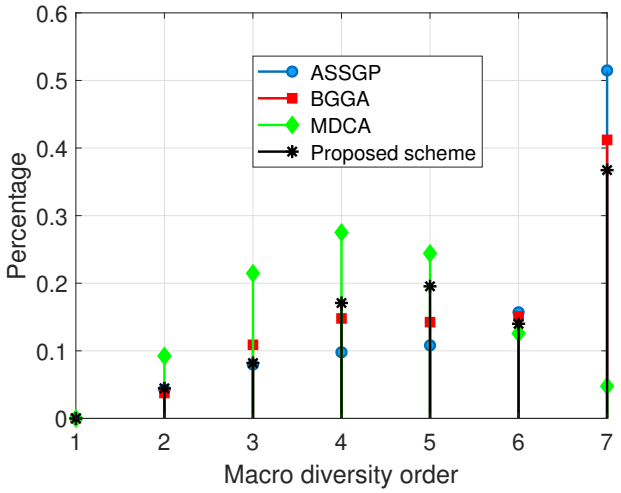

Fig. 8: Probabilities of the macro diversity orders for MDCA, ASSGA, BGGA, and the proposed scheme.

the CDF of the SINR lower bound $\overline{\text{SINR}}_{b,g}(\mathbf{y}^\star, \mathbf{X}^\star), \forall b, g$ in (10) is also plotted. It is observed that the MDCA reveals the best SINR performance due to the smallest number of deployed BSs (lower network interference level). However, this outpacing result is due to the ignorance of the physical and UE access-limited blockages, resulting in the worst UE outage performance as will be shown in Fig. 9. The proposed scheme, deploying 87 BSs, has a slightly larger number of the deployed BSs than the ASSGA (84 BSs) in Fig. 5, but has better SINR performance since ASSGA does not account for the SINR outdage during its deployment. The BGGA that deploys the largest number of BSs (i.e., 102 BSs) shows a worse SINR performance than that of the proposed scheme due to the increased network interference. The SINR outage for a connected link occurs when the SINR is lower than the threshold $z = 1$ in TABLE II. It is noticed from Fig. 7 that 77% of the links for the proposed scheme have the SINR lower bound $\overline{\text{SINR}}_{b,g}(\mathbf{y}^\star, \mathbf{X}^\star) \geq z = 1$ in (10), while 78% of the links have the true SINR $\text{SINR}_{b,g}(\mathbf{y}^\star, \mathbf{X}^\star) \geq z = 1$. Since the link with $\overline{\text{SINR}}_{b,g}(\mathbf{y}^\star, \mathbf{X}^\star) \geq z$ ensueres $\Pr\left(\overline{\text{SINR}}_{b,g}(\mathbf{y}^\star, \mathbf{X}^\star) < z | \mathbf{y}^\star, \mathbf{X}^\star\right) = \Pr\left(\text{SINR}_{b,g}(\mathbf{y}^\star, \mathbf{X}^\star) < z | \mathbf{y}^\star, \mathbf{X}^\star\right) = 0$, this reveals a tight SINR outage upper bound in (11).

5) Varying Number of Candidate BS Locations

In TABLE III, we present the results of the proposed BS deployment for different numbers of candidate BS locations as in Fig. 3(b) and for different sets of parameters. It can be observed that increasing the number of RF chains N_{RF} decreases the number of deployed BSs. This is because, given the UE access-limited blockage tolerance γ, a BS with a larger N_{RF} can cover more grids. Moreover, it is noticed that the number of candidate BS locations B also impact to the BS deployment results. When $N_{RF} = 14, \zeta_g = 0.1$ in TABLE III, two more BSs are deployed when $B = 184$ compared to the case when $B = 240$ due to the smaller search space for BS deployment. As we further reduce the number of candidate BS locations B, it raises the infeasibility issue of the proposed BS deployment scheme as shown in TABLE III. It is also observed that relaxing the UE outage tolerance substantially reduces the number of deployed BSs (also the cost) as well as improves the feasibility.

6) Macro Diversity Order Distribution

The macro diversity orders $\sum_{b \in \mathcal{B}} x_{b,g}, \forall g \in \mathcal{G}$ in (1) of each scheme are collected and $\Pr\left(\sum_b x_{b,g} = i\right)$ are presented in Fig. 8 for the deployment results in Fig. 5. Note that all schemes guarantee a minimum macro diversity order 2, which is a constraint for the MDCA and ASSGA, and an implicit requirement for the BGGA and proposed scheme. Without the UE access-limited blockage constraint, deployed BSs of MDCA can cover any LoS-visible grids within $R^{\max}$ and hence, it deploys the minimum number of BSs (i.e., 61 BSs) to produce the largest $\Pr\left(\sum_b x_{b,g} = i\right)$ at $i = 2, 3, 4, 5$ as seen in Fig. 8. While the proposed scheme has a similar (respectively, smaller) number of deployed BSs to the ASSGA (than the BGGA), its $\Pr\left(\sum_b x_{b,g} = i\right)$ at $i = 2, 3, 4, 5$ is larger than those of the ASSGA and BGGA, which demonstrates the superior performance of the proposed scheme compared to the benchmarks in terms of providing UE outage guarantees; this will be clear in Fig. 9.

7) UE Outage Probability

Based on the BS deployment results in Fig. 5, we collect the UE outage probabilities in (23f). The CDFs of the collected UE outage probabilities are demonstrated in Fig. 9. It is evident that the proposed scheme guarantees the UE outage probability with the specified tolerance $\zeta_g = 0.05, \forall g$ in TABLE II. Even through the ASSGA deploys the similar number of BSs as the proposed scheme, its UE outage performance is much worse than the proposed scheme and nearly 12% UEs have outage probability larger than 0.1. The BGGA exhibits the similar UE outage statistics to the proposed scheme. However, it fails to provides the guarantee and its performance is achieved by deploying 102 BSs.

TABLE III: Proposed BS deployment under different parameter settings.

Different B	Parameter setting	Number of BSs	Deployment cost
$B = 240$	$N_{RF} = 12$, $\zeta_g = 0.05$	87	46.4
$B = 240$	$N_{RF} = 14$, $\zeta_g = 0.05$	86	45.6
$B = 240$	$N_{RF} = 14$, $\zeta_g = 0.1$	82	44.6
$B = 184$	$N_{RF} = 12$, $\zeta_g = 0.05$	Infeasible	Not available
$B = 184$	$N_{RF} = 14$, $\zeta_g = 0.05$	Infeasible	Not available
$B = 184$	$N_{RF} = 14$, $\zeta_g = 0.1$	84	45.4
$B = 130$	$N_{RF} = 12$, $\zeta_g = 0.05$	Infeasible	Not available
$B = 130$	$N_{RF} = 14$, $\zeta_g = 0.1$	Infeasible	Not available
$B = 130$	$N_{RF} = 14$, $\zeta_g = 0.2$	50	23.2

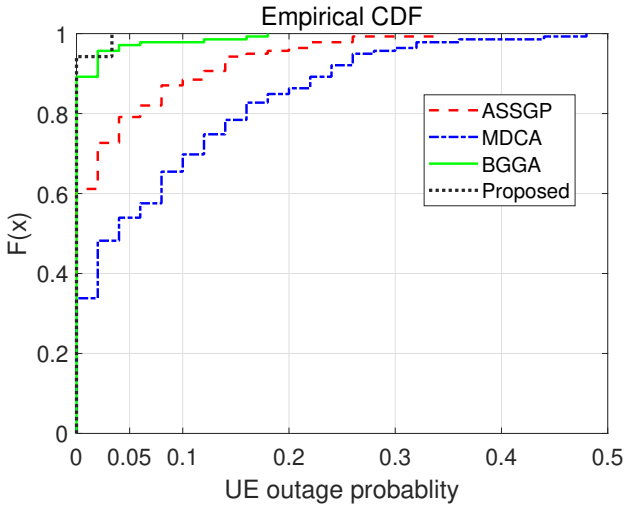

Fig. 9: CDF of the collected UE outage probabilities.

VII. Conclusions

We proposed a link quality-guaranteed minimum-cost mmWave BS deployment scheme that jointly optimizes the BS placement and cell coverage. To mathematically formulate the problem, we first introduced the stochastic mmWave link state model and analyzed the BS association and UE outage constraints. The BS deployment problem was then formulated as INP, which was suboptimally solved by decomposing it into two separable subproblems: (i) cell coverage optimization problem and (ii) minimum subset BS selection problem. We provided the solutions for these subproblems as well as their theoretical justifications. Simulation results demonstrated the efficacy of the proposed scheme in terms of the BS deployment cost, computational complexity, UE access-limited blockage, and UE outage performance. Compared to the benchmarks, our proposed algorithm provides guaranteed tolerance to UE access-limited blockage and UE outage.

It should be noted here that our main goal in this work was to study the principle of minimum-cost BS deployment for combined coverage and link quality constraints in mmWave networks, and through simulations describe the gain and the performance guarantee that can be expected by taking on such an approach. One major drawback of the proposed scheme was that the time complexity is exceedingly high compared to other benchmarks. However, considering the fact that the BS deployment planning is done off-line in practice, our proposed scheme optimally solves the INP in (23), and the proposed scheme provided stark outage guarantees, the high time complexity is not a serious drawback.

Acknowledgement

We are deeply indebted to the reviewers, whose consistent comments greatly improved the manuscript.

Appendix A
Proof of Lemma 1

Rewriting the logarithmic function in (16) as $\log(\Psi_{b,g})$ with $\Psi_{b,g} \triangleq p_{b,g}^{\text{blk}} + \rho_{b,g}(\mathbf{x}_b)\left(1 - p_{b,g}^{\text{blk}}\right) + \left(1-\rho_{b,g}(\mathbf{x}_b)\right)\widehat{p}_{b,g}^{\text{SINR}}(\mathbf{y}, \mathbf{X})$, $\log(\Psi_{b,g})$ is an increasing function of $\Psi_{b,g}$. Hence, we only need to show that the $\Psi_{b,g}$ is a monotonically increasing function of $\rho_{b,g}(\mathbf{x}_b)$. The first-order derivative of $\Psi_{b,g}$ with respect to $\rho_{b,g}(\mathbf{x}_b)$ is greater than or equal to zero, i.e.,

$$\frac{\partial \Psi_{b,g}}{\partial \rho_{b,g}(\mathbf{x}_b)} = \left(1 - p_{b,g}^{\text{blk}}\right) - \widehat{p}_{b,g}^{\text{SINR}}(\mathbf{y}, \mathbf{X}) \overset{(b)}{\geq} 0,$$

where (b) follows from the definition of $\widehat{p}_{b,g}^{\text{SINR}}(\mathbf{y}, \mathbf{X})$ in (13) and the upper bound

$$\widehat{p}_{b,g}^{\text{SINR}}(\mathbf{y}, \mathbf{X}) = \left(1-p_{b,g}^{\text{blk}}\right) \Pr\left(\overline{\text{SINR}}_{b,g}(\mathbf{y}, \mathbf{X}) z | \mathbf{y}, \mathbf{X}\right) \leq 1-p_{b,g}^{\text{blk}}, \tag{39}$$

which comletes the proof.

Appendix B
Proof of Lemma 2

The proof is equivalent to showing that the $\rho_{b,g}(\mathbf{x}_b)$ in (7) is a monotonically increasing function of $E[n_b(\mathbf{x}_b)]$, which can be verified by taking the first-order derivative of $\rho_{b,g}(\mathbf{x}_b)$

with respect to $E[n_b(\mathbf{x}_b)]$, yielding

$$\begin{aligned}\frac{\partial \rho_{b,g}(\mathbf{x}_b)}{\partial E[n_b(\mathbf{x}_b)]} &= \sum_{i=N_{\text{RF}}+1}^{+\infty} \frac{E[n_b(\mathbf{x}_b)]^{i-1}}{(i-1)!} e^{-E[n_b(\mathbf{x}_b)]} \frac{i-N_{\text{RF}}}{i} \\ &\quad - \sum_{i=N_{\text{RF}}+1}^{+\infty} \frac{E[n_b(\mathbf{x}_b)]^{i}}{i!} e^{-E[n_b(\mathbf{x}_b)]} \frac{i-N_{\text{RF}}}{i} \\ &\overset{(a)}{=} e^{-E[n_b(\mathbf{x}_b)]} \left(\frac{E[n_b(\mathbf{x}_b)]^{N_{\text{RF}}}}{(N_{\text{RF}}+1)!} + \sum_{i=N_{\text{RF}}+1}^{+\infty} \frac{E[n_b(\mathbf{x}_b)]^{i}}{i!} \left(\frac{N_{\text{RF}}}{i} - \frac{N_{\text{RF}}}{i+1} \right) \right) \\ &\geq \quad 0,\end{aligned}$$

where the step (a) follows from the fact that $\sum_{i=N_{\text{RF}}+1}^{+\infty} \frac{E[n_b(\mathbf{x}_b)]^{i-1}}{(i-1)!} e^{-E[n_b(\mathbf{x}_b)]} \frac{i-N_{\text{RF}}}{i}$ in the first equality can be rewritten as

$$e^{-E[n_b(\mathbf{x}_b)]} \frac{E[n_b(\mathbf{x}_b)]^{N_{\text{RF}}}}{(N_{\text{RF}}+1)!} + \sum_{i=N_{\text{RF}}+1}^{+\infty} \frac{E[n_b(\mathbf{x}_b)]^{i}}{i!} e^{-E[n_b(\mathbf{x}_b)]} \frac{i+1-N_{\text{RF}}}{i+1}.$$

This completes the proof.

Appendix C
Proof of Lemma 3

We first claim that the left-hanf-side of (23f) is non-positive, i.e.,

$$\log\Big(p_{b,g}^{\text{blk}} + \gamma\left(1 - p_{b,g}^{\text{blk}}\right) + (1-\gamma)\,\widehat{p}_{b,g}^{\text{SINR}}(\mathbf{y},\mathbf{X})\Big) \leq 0,$$

which can be checked by the bound

$$\begin{aligned}\widehat{p}_{b,g}^{\text{SINR}}(\mathbf{y},\mathbf{X}) &= \left(1-p_{b,g}^{\text{blk}}\right)\Pr\Big(\overline{\text{SINR}}_{b,g}(\mathbf{y},\mathbf{X}) < z|\mathbf{y},\mathbf{X}\Big) \quad (40)\\ &\leq 1-p_{b,g}^{\text{blk}}.\end{aligned}$$

This reveals that if $\widehat{p}_{b,g}^{\text{SINR}}(\mathbf{y},\mathbf{X})$ in (40) (defined in (14)) is a monotonically decreasing function of the diversity order $\sum_{b\in\mathcal{B}} x_{b,g}$, so is the left-hand-side of (23f). Thus, in what follows, it suffices to show the monotonicity of $\widehat{p}_{b,g}^{\text{SINR}}(\mathbf{y},\mathbf{X})$. To this end, we divide the proof into two cases when $x_{b,g}=1$ and $x_{b,g}=0$.

First, when $x_{b,g}=1$, it can be shown from (9) and (10) that as the macro diversity order $\sum_{b\in\mathcal{B}} x_{b,g}$ of a UE in grid g increases for a fixed $\mathbf{y}$, the composite interference power $\sum_{i\in\mathcal{B}} y_i \widehat{I}_{i,g}(x_{i,g})$ decreases, concluding that $\widehat{p}_{b,g}^{\text{SINR}}(\mathbf{y},\mathbf{X})$ is a monotonically decreasing function of $\sum_{b\in\mathcal{B}} x_{b,g}$. On the other hand, when $x_{b,g}=0$, the increment of macro diversity order $\sum_{b\in\mathcal{B}} x_{b,g}$ can lead to either $x_{b,g}=0$ (unchanged) or $x_{b,g}=1$. In the former case, we have $\widehat{p}_{b,g}^{\text{SINR}}(\mathbf{y},\mathbf{X}) = 1-p_{b,g}^{\text{blk}}$ due to (8), while in the latter case, $\widehat{p}_{b,g}^{\text{SINR}}(\mathbf{y},\mathbf{X})$ decreases, i.e., $\widehat{p}_{b,g}^{\text{SINR}}(\mathbf{y},\mathbf{X}) \leq 1-p_{b,g}^{\text{blk}}$. As a result, we conclude that $\widehat{p}_{b,g}^{\text{SINR}}(\mathbf{y},\mathbf{X})$ is a monotonically decreasing function of $\sum_{b\in\mathcal{B}} x_{b,g}$. This completes the proof.

Appendix D
Proof of Lemma 4

It is not difficult to observe that if $y_b\Lambda_{b,g}^{\star}=1$, the $s_{b,g}$ in (33) is either $s_{b,g}=0$ or $s_{b,g}=1$, while if $y_b\Lambda_{b,g}^{\star}=0$, then $s_{b,g}=0$, leading to

$$s_{b,g} \leq y_b\Lambda_{b,g}^{\star}, \quad s_{b,g}\in\{0,1\}. \tag{41}$$

Because $M_{b,g} > \sigma^2 + \sum_{i\in\mathcal{B}} y_i \widehat{I}_{i,g}(\Lambda_{i,g}^{\star})$, the indicator function in (33) can be equivalently expressed as the following two linear equations:

$$\sigma^2 + \sum_{i\in\mathcal{B}} y_i \widehat{I}_{i,g}(\Lambda_{b,g}^{\star}) \geq \frac{y_b \overline{P}_{b,g}(\Lambda_{b,g}^{\star})}{z} - s_{b,g}M_{b,g} \tag{42}$$

and

$$\sigma^2 + \sum_{i\in\mathcal{B}} y_i \widehat{I}_{i,g}(\Lambda_{b,g}^{\star}) < \frac{y_b \overline{P}_{b,g}(\Lambda_{b,g}^{\star})}{z} + (1-s_{b,g})M_{b,g}. \tag{43}$$

For the $s_{b,g}$ satisfying (41)-(43), the $\widehat{p}_{b,g}^{\text{SINR}}$ in (31) can be simplified to

$$\tilde{p}_{b,g}^{\text{SINR}} = \left(1-p_{b,g}^{\text{blk}}\right)\left(1-s_{b,g}\right). \tag{44}$$

Plugging (44) in the term $\log(p_{b,g}^{\text{blk}} + \gamma(1-p_{b,g}^{\text{blk}}) + (1-\gamma)\tilde{p}_{b,g}^{\text{SINR}}(\mathbf{y}))$ on the left-hand-side of (32b) and incorporating the two cases, $s_{b,g}=0$ and $s_{b,g}=1$, into it lead to

$$s_{b,g}\log\Big(p_{b,g}^{\text{blk}} + \gamma(1-p_{b,g}^{\text{blk}})\Big). \tag{45}$$

Therefore the UE outage constraint in (32b) is succinctly

$$\sum_{b\in\mathcal{B}} y_b\Lambda_{b,g}^{\star} s_{b,g} \log\Big(p_{b,g}^{\text{blk}} + \gamma(1-p_{b,g}^{\text{blk}})\Big) \leq \log\left(\zeta_g\right),\ \forall g\in\mathcal{G},$$

which is still nonlinear with respect to the variables y_b and $s_{b,g}$ because they are coupled. However, $s_{b,g} \leq y_b\Lambda_{b,g}^{\star}$ in (41) implies

$$s_{b,g} = y_b\Lambda_{b,g}^{\star} s_{b,g}, \tag{46}$$

which is obtained by multiplying $s_{b,g}$ to the both sides of (41). The linearized UE outage constraint is then given by

$$\sum_{b\in\mathcal{B}} s_{b,g}\log\Big(p_{b,g}^{\text{blk}} + \gamma(1-p_{b,g}^{\text{blk}})\Big) \leq \log\left(\zeta_g\right),\ \forall g\in\mathcal{G}. \tag{47}$$

In summary, the nonlinear constraint (32b) can be replaced by the linear constraints (41)-(43) and (47), which completes the proof.

References

[1] S. Hur, T. Kim, D. J. Love, J. V. Krogmeier, T. A. Thomas, and A. Ghosh, "Millimeter wave beamforming for wireless backhaul and access in small cell networks," *IEEE Transactions on Communications*, vol. 61, no. 10, pp. 4391–4403, Oct. 2013.

[2] B. P. S. Sahoo, C. Chou, C. Weng, and H. Wei, "Enabling millimeter-wave 5G networks for massive IoT applications: A closer look at the issues impacting millimeter-waves in consumer devices under the 5G framework," *IEEE Consumer Electronics Magazine*, vol. 8, no. 1, pp. 49–54, Jan 2019.

[3] V. Raghavan, A. Partyka, A. Sampath, S. Subramanian, O. H. Koymen, K. Ravid, J. Cezanne, K. Mukkavilli, and J. Li, "Millimeter-wave MIMO prototype: Measurements and experimental results," *IEEE Communications Magazine*, vol. 56, no. 1, pp. 202–209, Jan 2018.

[4] T. S. Rappaport, Y. Xing, G. R. MacCartney, A. F. Molisch, E. Mellios, and J. Zhang, "Overview of millimeter wave communications for fifth-generation (5G) wireless networks—with a focus on propagation models," *IEEE Transactions on Antennas and Propagation*, vol. 65, no. 12, pp. 6213–6230, 2017.

[5] T. Bai, R. Vaze, and R. W. Heath, "Analysis of blockage effects on urban cellular networks," *IEEE Transactions on Wireless Communications*, vol. 13, no. 9, pp. 5070–5083, Sep. 2014.

[6] H. Zhao, R. Mayzus, S. Sun, M. Samimi, J. K. Schulz, Y. Azar, K. Wang, G. N. Wong, F. Gutierrez, and T. S. Rappaport, "28 ghz millimeter wave cellular communication measurements for reflection and penetration loss

in and around buildings in new york city," in *2013 IEEE International Conference on Communications (ICC)*, 2013, pp. 5163–5167.

[7] U. T. Virk and K. Haneda, "Modeling human blockage at 5g millimeter-wave frequencies," *IEEE Transactions on Antennas and Propagation*, vol. 68, no. 3, pp. 2256–2266, 2020.

[8] R. W. Heath, N. González-Prelcic, S. Rangan, W. Roh, and A. M. Sayeed, "An overview of signal processing techniques for millimeter wave MIMO systems," *IEEE Journal of Selected Topics in Signal Processing*, vol. 10, no. 3, pp. 436–453, 2016.

[9] H. Ghauch, T. Kim, M. Bengtsson, and M. Skoglund, "Subspace estimation and decomposition for large millimeter-wave MIMO systems," *IEEE Journal of Selected Topics in Signal Processing*, vol. 10, no. 3, pp. 528–542, April 2016.

[10] A. Alkhateeb, R. W. Heath, and G. Leus, "Achievable rates of multi-user millimeter wave systems with hybrid precoding," in *2015 IEEE International Conference on Communication Workshop (ICCW)*, Jun. 2015, pp. 1232–1237.

[11] W. Zhang, T. Kim, D. J. Love, and E. Perrins, "Leveraging the restricted isometry property: Improved low-rank subspace decomposition for hybrid millimeter-wave systems," *IEEE Transactions on Communications*, vol. 66, no. 11, pp. 5814–5827, Nov 2018.

[12] O. E. Ayach, S. Rajagopal, S. Abu-Surra, Z. Pi, and R. W. Heath, "Spatially sparse precoding in millimeter wave MIMO systems," *IEEE Transactions on Wireless Communications*, vol. 13, no. 3, pp. 1499–1513, Mar. 2014.

[13] A. Alkhateeb, O. E. Ayach, G. Leus, and R. W. Heath, "Channel estimation and hybrid precoding for millimeter wave cellular systems," *IEEE Journal of Selected Topics in Signal Processing*, vol. 8, no. 5, pp. 831–846, Oct. 2014.

[14] M. Dong and T. Kim, "Interference analysis for millimeter-wave networks with geometry-dependent first-order reflections," *IEEE Transactions on Vehicular Technology*, vol. 67, no. 12, pp. 12 404–12 409, Dec. 2018.

[15] J. Choi, "On the macro diversity with multiple BSs to mitigate blockage in millimeter-wave communications," *IEEE Communications Letters*, vol. 18, no. 9, pp. 1653–1656, Sep. 2014.

[16] A. Alizadeh and M. Vu, "Time-fractional user association in millimeter wave MIMO networks," in *2018 IEEE International Conference on Communications (ICC)*, May 2018, pp. 1–6.

[17] H. Zhang, S. Huang, C. Jiang, K. Long, V. C. M. Leung, and H. V. Poor, "Energy efficient user association and power allocation in millimeter-wave-based ultra dense networks with energy harvesting base stations," *IEEE Journal on Selected Areas in Communications*, vol. 35, no. 9, pp. 1936–1947, Sep. 2017.

[18] (2019, Oct) Precision planning for 5G era network with smallcells, white paper. [Online]. Available: https://www.scf.io/en/documents/230_Precision_planning_for_5G_Era_networks_with_small_cells.php

[19] J. Peng, P. Hong, and K. Xue, "Energy-aware cellular deployment strategy under coverage performance constraints," *IEEE Transactions on Wireless Communications*, vol. 14, no. 1, pp. 69–80, Jan. 2015.

[20] G. Zhao, S. Chen, L. Zhao, and L. Hanzo, "Joint energy-spectral-efficiency optimization of CoMP and BS deployment in dense large-scale cellular networks," *IEEE Transactions on Wireless Communications*, vol. 16, no. 7, pp. 4832–4847, Jul. 2017.

[21] B. Yang, G. Mao, X. Ge, M. Ding, and X. Yang, "On the energy-efficient deployment for ultra-dense heterogeneous networks with NLoS and LoS transmissions," *IEEE Transactions on Green Communications and Networking*, vol. 2, no. 2, pp. 369–384, Jun. 2018.

[22] P. Mekikis, E. Kartsakli, A. Antonopoulos, A. S. Lalos, L. Alonso, and C. Verikoukis, "Two-tier cellular random network planning for minimum deployment cost," in *IEEE International Conference on Communications*, Jun. 2014, pp. 1248–1253.

[23] C. Peng, L. Wang, and C. Liu, "Optimal base station deployment for small cell networks with energy-efficient power control," in *2015 IEEE International Conference on Communications (ICC)*, Jun. 2015, pp. 1863–1868.

[24] M. Dong, T. Kim, J. Wu, and E. W. M. Wong, "Cost-efficient millimeter wave base station deployment in manhattan-type geometry," *IEEE Access*, vol. 7, pp. 149 959–149 970, 2019.

[25] S. Chatterjee, M. J. Abdel-Rahman, and A. B. MacKenzie, "Optimal base station deployment with downlink rate coverage probability constraint," *IEEE Wireless Communications Letters*, vol. 7, no. 3, pp. 340–343, Jun. 2018.

[26] C. Fan, T. Zhang, and Z. Zeng, "Energy-efficient base station deployment in HetNet based on traffic load distribution," in *2017 IEEE 85th Vehicular Technology Conference (VTC Spring)*, Jun. 2017, pp. 1–5.

[27] M. A. Yigitel, O. D. Incel, and C. Ersoy, "Dynamic BS topology management for green next generation HetNets: An urban case study," *IEEE Journal on Selected Areas in Communications*, vol. 34, no. 12, pp. 3482–3498, Dec. 2016.

[28] C. C. Coskun and E. Ayanoglu, "Energy-efficient base station deployment in heterogeneous networks," *IEEE Wireless Communications Letters*, vol. 3, no. 6, pp. 593–596, Dec. 2014.

[29] Y. Lu, H.-W. Hsu, and L.-C. Wang, "Performance model and deployment strategy for mm-wave multi-cellular systems," in *2016 25th Wireless and Optical Communication Conference*, May 2016, pp. 1–4.

[30] S. S. Szyszkowicz, A. Lou, and H. Yanikomeroglu, "Automated placement of individual millimeter-wave wall-mounted base stations for line-of-sight coverage of outdoor urban areas," *IEEE Wireless Communications Letters*, vol. 5, no. 3, pp. 316–319, Jun. 2016.

[31] N. Palizban, S. Szyszkowicz, and H. Yanikomeroglu, "Automation of millimeter wave network planning for outdoor coverage in dense urban areas using wall-mounted base stations," *IEEE Wireless Communications Letters*, vol. 6, no. 2, pp. 206–209, Apr. 2017.

[32] M. Gonzalez and J. Thompson, "An energy efficient base station deployment for mmWave based wireless backhaul," in *2016 IEEE 27th Annual International Symposium on Personal, Indoor, and Mobile Radio Communications (PIMRC)*, Sep. 2016, pp. 1–6.

[33] Y. Zhang, L. Dai, and E. W. M. Wong, "Optimal BS deployment and user association for 5G millimeter wave communication networks," *IEEE Transactions on Wireless Communications*, vol. 20, no. 5, pp. 2776–2791, 2021.

[34] I. Mavromatis, A. Tassi, R. J. Piechocki, and A. R. Nix, "Efficient millimeter-wave infrastructure placement for city-scale ITS," *CoRR*, vol. abs/1903.01372, 2019. [Online]. Available: http://arxiv.org/abs/1903.01372

[35] M. Naderi Soorki, W. Saad, and M. Bennis, "Optimized deployment of millimeter wave networks for in-venue regions with stochastic users' orientation," *IEEE Transactions on Wireless Communications*, vol. 18, no. 11, pp. 5037–5049, 2019.

[36] M. Dong, T. Kim, J. Wu, and W. M. E. Wong, "Millimeter-wave base station deployment using the scenario sampling approach," *IEEE Transactions on Vehicular Technology*, vol. 69, no. 11, pp. 14 013–14 018, 2020.

[37] K. Shen, Y. Liu, D. Y. Ding, and W. Yu, "Flexible multiple base station association and activation for downlink heterogeneous networks," *IEEE Signal Processing Letters*, vol. 24, no. 10, pp. 1498–1502, Oct. 2017.

[38] M. Feng, S. Mao, and T. Jiang, "BOOST: Base station on-off switching strategy for green massive MIMO hetnets," *IEEE Transactions on Wireless Communications*, vol. 16, no. 11, pp. 7319–7332, Nov. 2017.

[39] X. Lin and S. Wang, "Joint user association and base station switching on/off for green heterogeneous cellular networks," in *2017 IEEE International Conference on Communications (ICC)*, May 2017, pp. 1–6.

[40] J. Kim, W. S. Jeon, and D. G. Jeong, "Base-station sleep management in open-access femtocell networks," *IEEE Transactions on Vehicular Technology*, vol. 65, no. 5, pp. 3786–3791, May 2016.

[41] M. Dong, W. Chan, T. Kim, K. Liu, H. Huang, and G. Wang, "Simulation study on millimeter wave 3D beamforming systems in urban outdoor multi-cell scenarios using 3D ray tracing," in *IEEE 26th Annual International Symposium on PIMRC*, Aug. 2015, pp. 2265–2270.

[42] G. T. 38.211. (2020, Jan.) Physical channels and modulation. [Online]. Available: https://portal.3gpp.org/desktopmodules/Specifications/SpecificationDetails.aspx?specificationId=3213

[43] T. S. Rappaport, S. Sun, R. Mayzus, H. Zhao, Y. Azar, K. Wang, G. N. Wong, J. K. Schulz, M. Samimi, and F. Gutierrez, "Millimeter wave mobile communications for 5G cellular: It will work!" *IEEE Access*, vol. 1, pp. 335–349, May 2013.

[44] T. Bai and R. W. Heath, "Coverage and rate analysis for millimeter-wave cellular networks," *IEEE Transactions on Wireless Communications*, vol. 14, no. 2, pp. 1100–1114, Feb. 2015.

[45] M. D. Renzo, "Stochastic geometry modeling and analysis of multi-tier millimeter wave cellular networks," *IEEE Transactions on Wireless Communications*, vol. 14, no. 9, pp. 5038–5057, Sep. 2015.

[46] J. Vales-Alonso, F. Parrado-García, P. López-Matencio, J. Alcaraz, and F. González-Castaño, "On the optimal random deployment of wireless sensor networks in non-homogeneous scenarios," *Ad Hoc Networks*, vol. 11, no. 3, pp. 846–860, 2013.

[47] M. Haenggi, "Stochastic geometry for wireless networks," *Cambridge, U.K.: Cambridge Univ. Press*, 2012.

[48] M. Dong, W. Chan, T. Kim, K. Liu, H. Huang, and G. Wang, "Simulation study on millimeter wave 3D beamforming systems in urban outdoor multi-cell scenarios using 3D ray tracing," in *2015 IEEE 26th*

Annual International Symposium on Personal, Indoor, and Mobile Radio Communications (PIMRC), Aug 2015, pp. 2265–2270.

[49] R. L. Strei, *Poisson Point Processess: Imaging, Tracking, and Sensing*. Springer US, Sep. 2010.

[50] D. Li and X. Sun, *Nonlinear Integer Programming*. Springer US, 2006.

[51] Gurobi. (2018) Gurobi optimier quick start guide. [Online]. Available: https://www.gurobi.com/wp-content/plugins/hd_documentations/content/pdf/quickstart_windows_8.1.pdf

[52] G. R. MacCartney and T. S. Rappaport, "Millimeter-wave base station diversity for 5g coordinated multipoint (CoMP) applications," *IEEE Transactions on Wireless Communications*, vol. 18, no. 7, pp. 3395–3410, 2019.

[53] L. Encyclopedia. (2021) LTE radio link budgeting and RF planning. [Online]. Available: https://sites.google.com/site/lteencyclopedia/lte-radio-link-budgeting-and-rf-planning